

2. SYSTEMS STUDIES

Ronald L. Miller

Robert A. Krakowski

David A. Ehst

Contents

2.1.	INTRODUCTION	2-1
2.2.	MODELS AND METHODS	2-3
2.2.1.	Plasma Engineering Model	2-3
2.2.2.	Reactor Engineering Model	2-12
2.3.	COSTING AND ECONOMICS	2-19
2.4.	DESIGN POINT DETERMINATION	2-33
2.4.1.	Safety Factor Variation: Beta <i>vs</i> Magnetic Field	2-33
2.4.2.	Temperature Variation: Current-Drive Power <i>vs</i> Fusion Power	2-38
2.4.3.	Parametric Results	2-43
2.4.4.	ARIES-I Reference Design	2-50
2.5.	CRITICAL ISSUES	2-57
2.6.	SUMMARY AND CONCLUSIONS	2-57
	REFERENCES	2-59

2. SYSTEMS STUDIES

2.1. INTRODUCTION

The objective of the systems analysis activity is the systematic study and determination of plant operating parameters through economic analysis and optimization of the power station, emphasizing the performance of the fusion power core. The fusion power core (FPC) includes the tokamak plasma chamber, first wall, blanket, shield, coils, and associated structure. The reference design points are chosen to meet overall design goals of the ARIES-I study, such as minimal cost of electricity (COE, mill/kWh) and high mass power density (MPD, kWe/tonne). In addition, trade-off and sensitivity studies were performed to establish and characterize the design window for attractive tokamak reactors. Results and constraints from detailed modeling and engineering design effort are fed back and integrated into the systems model. The systems code, therefore, is used as a tool in the iterative conceptual engineering-design process.

The ARIES systems code evolved from a systems code used to model the spherical-torus tokamak [1] and from the reversed-field-pinch systems code used in the TITAN study [2]. The ARIES systems code includes a physics model comparable to that of the MUMAK code [3, 4], which is used for U.S. ITER [5] modeling. Informal benchmarking with the TRAC-II code [6, 7] (physics and engineering), the European SUPERCOIL/SCAN codes [8] (physics, engineering, and costing), and the GENEROMAK code [9, 10] (physics, engineering, and costing) has been performed with generally satisfactory results [11].

The overall features and logic of the ARIES systems code are schematically given in Fig. 2.1-1. The systems code incorporates a series of computational search loops (*e.g.*, fixed aspect ratio and variable minor radius), which solve for the FPC physics and engineering characteristics. Subject to certain constraints and design goals, cost dependencies are identified, and the key interactions between system variables are determined. Design points identified by this procedure are subjected to detailed analysis and subsystem design, with conceptual design results being fed back to the systems design code throughout the project for further optimization and refinement. Ongoing calibrations with separate subsystem models used in the project are made. Results of plasma engineering, blanket and shield, impurity control, magnet, power conversion, maintenance, tritium handling, safety, and other analyses are integrated, sometimes in approximate form, into

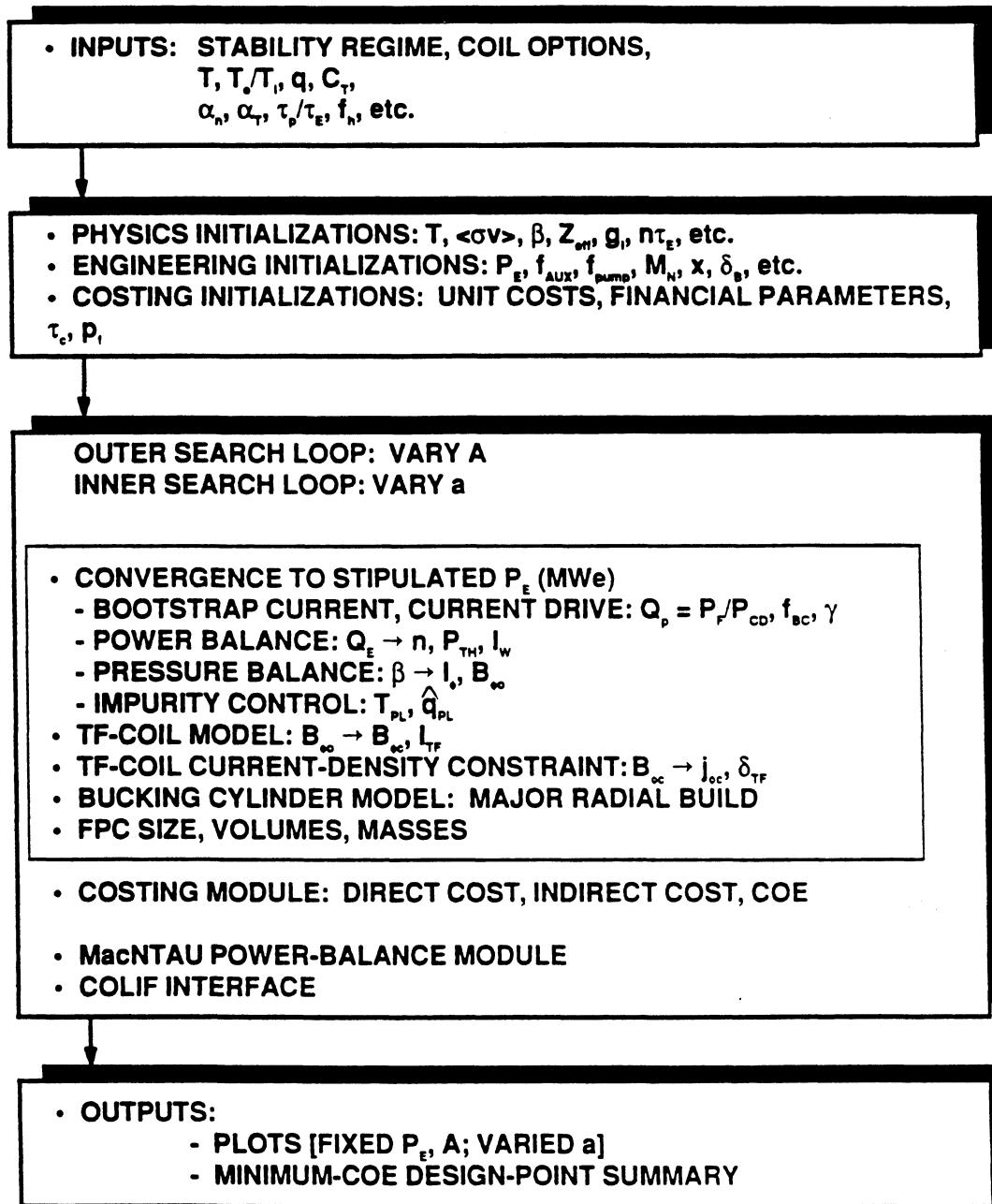


Figure 2.1-1. ARIES systems-code logic and flow diagram, combining plasma engineering, technology, and costing modules. The MacNTAU [12] power-balance solver is incorporated in the systems code directly. An input file for the separate COLIF code [13-15] (modeling aspects which emphasize the kinetics) is generated for physics modeling.

the systems optimization model, which typically uses COE as the object function to be minimized.

Section 2.2 summarizes the physics and engineering models used in the ARIES systems code. Section 2.3 describes the costing and economics assumptions and algorithms used to project COE estimates. The results of parametric studies leading to the ARIES-I reference design point are discussed in Sec. 2.4. Summary and conclusions are given in Sec. 2.5.

2.2. MODELS AND METHODS

2.2.1. Plasma Engineering Model

The ARIES systems-code model for plasma engineering begins with a steady-state, point-plasma model that is corrected for profile effects. The toroidal plasma geometry is described by the major toroidal radius, R_T , and minor radius, a (*i.e.*, half width at the mid-plane), and vertical half height, b . The plasma aspect ratio is $A \equiv R_T/a = 1/\epsilon$. When needed, parameters at the separatrix surface are denoted by subscript \times (*e.g.*, κ_\times) and at the 95% flux surface by subscript 95 (*e.g.*, κ_{95}). In addition to the vertical elongation, $\kappa \equiv b/a$, the plasma poloidal boundary is also characterized by the triangularity parameter, δ . The plasma shape factor, S , which is the ratio of the plasma poloidal perimeter to the perimeter of a circular plasma ($\kappa = 1$) with the same value of minor radius, a , can be approximated by [16]

$$S = \oint \frac{\phi dl}{2\pi a} \Big|_{\psi_{edge}} \simeq \left[\frac{1 + \kappa^2 (1 + 2\delta^2 - 1.2\delta^3)}{2} \right]^{1/2}, \quad (2.2-1)$$

as representative of the more refined model [17] actually used in the ARIES systems code. The plasma cross-sectional area is given by [7]

$$A_p = \pi a^2 \kappa \left[\frac{2J_1(\delta)}{\delta} \right] \equiv \pi r_p^2, \quad (2.2-2)$$

where $J_1(x)$ is the first-order Bessel function of the first kind and r_p is the circularized (average) plasma radius. The corresponding major toroidal radius of the centroid of the plasma cross section is approximated by [7]

$$R'_T = R_T \left(1 - \frac{0.233 \delta}{A} \right), \quad (2.2-3)$$

such that the plasma volume is $V_p \equiv 2\pi R'_T A_p$. Then,

$$V_p = 2\pi^2 R_T a^2 \kappa \left(1 - \frac{0.233 \delta}{A}\right) \left[\frac{2J_1(\delta)}{\delta}\right]. \quad (2.2-4)$$

The plasma ion and electron densities are denoted by n_i and n_e , respectively. Local charge neutrality requires that

$$n_e(r) = \sum_j n_j(r) Z_j, \quad (2.2-5)$$

where the summation is over all ion species. The effective plasma charge is

$$Z_{eff} = \frac{\sum_j n_j Z_j^2}{\sum_j n_j Z_j}. \quad (2.2-6)$$

The ion population comprises deuterium (D) and tritium (T) as the primary fuel species, as well as fusion-product α -particles, proton (p), and ^3He (from the DD reactions), and impurities (*e.g.*, 1% O_2). The concentration of each ion species is $f_j \equiv n_j/n_i$, and inputs to the systems code are iterated with results of the COLIF code [13-15] for self-consistency. The central (peak) plasma temperature is $T(0) \equiv T_o$, and the central (peak) plasma density is $n(0) \equiv n_o$. The radial profiles of electric and ion temperatures and densities are approximated, respectively, by

$$T(r) = T_o \left[1 - \left(\frac{r}{r_p}\right)^2\right]^{\alpha_T}, \quad (2.2-7)$$

$$n(r) = n_s + (n_o - n_s) \left[1 - \left(\frac{r}{r_p}\right)^2\right]^{\alpha_n^*}, \quad (2.2-8)$$

where n_s is the separatrix (edge) density representative of a pedestal in the density profile. The value of the temperature profile exponent is $\alpha_T = 1.1$ and the value of the density profile exponent is $\alpha_n^* = 1.3$, yielding an n/n_o ratio similar to that of a density profile without a pedestal (*i.e.*, $n_s = 0$) with $\alpha_n = 0.3$. The plasma internal energy is

$$W_p = 1.5 k_B \left(n_e T_e + \sum_j n_j T_j\right), \quad (2.2-9)$$

where k_B is the Boltzmann constant.

The volume-averaged current density, plasma density, temperature, and density-weighted volume-averaged temperature are defined, respectively, as follows:

$$\begin{aligned}
 j_\phi &\equiv \frac{I_\phi}{A_p}, \\
 n &\equiv \frac{2\pi}{A_p} \int_0^{r_p} n(r) r dr, \\
 \bar{T} &\equiv \frac{2\pi}{A_p} \int_0^{r_p} T(r) r dr, \\
 T &\equiv \frac{2\pi}{n A_p} \int_0^{r_p} T(r) n(r) r dr,
 \end{aligned} \tag{2.2-10}$$

where I_ϕ is the toroidal plasma current. For a density profile with no pedestal ($n_s = 0$), these integrations yield:

$$\begin{aligned}
 \frac{n}{n_o} &= \frac{1}{1 + \alpha_n}, \\
 \frac{\bar{T}}{T_o} &= \frac{1}{1 + \alpha_T}, \\
 \frac{T}{T_o} &= \frac{1 + \alpha_n}{1 + \alpha_n + \alpha_T}.
 \end{aligned} \tag{2.2-11}$$

Also, the plasma pressure would have the same radial profile as given by Eq. (2.2-7) but with the exponent $\alpha_p \equiv \alpha_n + \alpha_T$.

The plasma surface-averaged poloidal magnetic field, $B_\theta \equiv \bar{B}_\theta(r_p)$, is produced by the toroidal current, I_ϕ , and the external poloidal-field coils and is given by

$$B_\theta = \frac{\oint B_\theta dl}{\oint dl} = \frac{\mu_o I_\phi}{2\pi a S}, \tag{2.2-12}$$

where μ_o is the permeability of the vacuum. The toroidal magnetic field, produced by external TF coils, provides the primary confining field in a tokamak. The on-axis toroidal magnetic-field strength is $B_\phi(R_T) \equiv B_{\phi o}$, the toroidal beta is $\beta \equiv 2\mu_o p / B_{\phi o}^2$, and the poloidal beta is $\beta_\theta \equiv 2\mu_o p / B_\theta^2$. The edge safety factor, q , is approximated by [16, 19]

$$q = 5C_q \frac{B_{\phi o} a}{I_\phi} \frac{\epsilon}{(1 - \epsilon^2)^2} S^2, \tag{2.2-13}$$

where the coefficient $C_q \equiv C_q(\epsilon\beta_\theta, q) \approx 1$ and I_ϕ is in MA. The toroidal and poloidal beta values are related by [19]

$$\beta = \beta_\theta \left[\frac{C_q}{q} \frac{\epsilon}{(1 - \epsilon^2)^2} \right]^2 S^2. \tag{2.2-14}$$

The ARIES-I plasma operates in the first stability regime. Therefore, the toroidal beta is taken to be limited by the Troyon relation [20],

$$\beta = C_T \frac{I_\phi}{a B_{\phi_0}}. \quad (2.2-15)$$

The ARIES-I reference MHD equilibrium is computed based on pressure and toroidal current-density profiles that are consistent with current-drive, transport, and impurity-control/particle-exhaust analyses. Values of plasma vertical elongation, κ_x , approaching 2 are desirable in increasing plasma volume and fusion power. A base-case value of $\kappa_x = 1.8$, however, is chosen based on the vertical stability analysis for ARIES-I and on the desire to place the passive stabilization elements behind the blanket. The values of on-axis safety factor, $q_o \sim 1.3$, and average plasma-edge safety factor, $q \sim 4.75$, reflect the trade-offs between equilibrium and stability analyses and the effort to maximize the bootstrap-current fraction. The base-case toroidal beta is 1.9% (corresponding to $C_T = 0.032$ T m/MA) and is found from high- n ballooning and $n = 1$ kink stability analyses of the ARIES-I equilibrium. Details of the plasma equilibrium and stability modeling are discussed in Sec. 3.

The steady-state plasma power balance equates the input power (*i.e.*, the charged-particle fusion power, P_α , absorbed current-drive power, P_{CD} , and ohmic power, P_Ω) with the radiative and transport power losses to give

$$P_\alpha + P_{CD} + P_\Omega = P_{BR} + P_{CY} + P_{TR}. \quad (2.2-16)$$

The two primary radiation-loss channels are bremsstrahlung and cyclotron radiation. The electron-ion and electron-electron bremsstrahlung local power density (W/m³) is generally given by [21]

$$P_{BR} = 5.35 \times 10^{-37} n_e^2 T_e^{1/2} \left[Z_{eff} \left(1 + 1.55 \times 10^{-3} T_e + 7.15 \times 10^{-6} T_e^2 \right) + 4.14 \times 10^{-3} T_e \right], \quad (2.2-17)$$

which includes correction for relativistic effects that tend to be significant only at temperatures above the typical ARIES-I operating point at $T \simeq 20$ keV. The cyclotron-(synchrotron) radiation global power density (W/m³) is given by [21]

$$P_{CY} = 6.214 \times 10^{-17} n_e T_e B_\phi^2 \Phi, \quad (2.2-18)$$

where the Trubnikov absorption correction is given by [21],

$$\Phi = \frac{5.198 \times 10^{-3}}{\Lambda^{1/2}} T_e^{1.5} \left(1 + \frac{22.61}{A T_e^{1/2}} \right)^{1/2} (1 - R_{CY})^{1/2}, \quad (2.2-19)$$

$$\Lambda^{1/2} = 7.78 \times 10^{-9} \left(\frac{n_e a}{B_\phi} \right)^{1/2}. \quad (2.2-20)$$

In the above expressions, the usual substitution ($B_\phi = B_{\phi o} \sqrt{1 - \beta}$) is made to correct for plasma diamagnetism. The reflectivity of the first wall, without holes, was estimated by Krajcik [22] to be

$$R_{CY}^K = 1 - \sqrt{2 \epsilon_o Z^* \omega_c \rho}, \quad (2.2-21)$$

where ϵ_o is the permittivity of the vacuum, ω_c is the electron cyclotron frequency, $Z^* \simeq 0.32T_e + 11.6$ {cf., Fig. 5 of Ref. [22]} represents the effective harmonic, and ρ is the electrical resistivity of the first-wall material. A correction to this expression to account for holes in the first wall was suggested by Schaffer [23]

$$R_{CY}^S = (1 - f_h) R_{CY}^K, \quad (2.2-22)$$

where f_h is the fraction of the first-wall surface area devoted to holes. Krajcik [22] also provides a more accurate expression for synchrotron radiation (without holes). Denoting Krajcik's accurate expression by K_c , defining K_ℓ from Trubnikov Eq. (2.2-21) through $\Phi = K_\ell \sqrt{1 - R_{CY}}$, and limiting $K_c < K_\ell$, Werley [24] has proposed the hole-corrected effective reflectivity,

$$R_{CY}^W = (1 - f_h) - (1 - f_h) \left(\frac{K_c}{K_\ell} \right)^2. \quad (2.2-23)$$

This expression is found to be more suitable for the poorly reflecting SiC-composite first wall used in ARIES-I. It should be noted that a number of similar models exist and that they produce various results [21], depending, for example, on the treatment of plasma profiles. Therefore, the simplified cyclotron-radiation model of Eq. (2.2-23) must be viewed as an approximation to future calculations using more refined codes [25]. The plasma-core radiation fraction is

$$f_{RAD} \equiv \frac{P_{BR} + P_{CY}}{P_\alpha + P_{CD} + P_\Omega}. \quad (2.2-24)$$

Generally, the volume-averaged power densities are given by

$$P_k \equiv \langle P_k(r) \rangle = \langle f_k[B(r), j(r), n(r), T(r)] \rangle, \quad (2.2-25)$$

where the subscript k denotes fusion, radiation, or ohmic-heating power density. The systems model calculates volume-averaged power densities, P_k , using averaged parameters; all profile information is contained in the profile-enhancement factors, g_k , where

$$P_k = g_k f_k(\langle B \rangle, \langle j \rangle, \langle n \rangle, \langle T \rangle). \quad (2.2-26)$$

Henceforth, these quantities are volume-averaged and the notation $\langle \cdot \rangle$ is dropped, except as otherwise specified, for simplicity. The profile factors are then defined as

$$g_k \equiv \frac{2\pi}{P_k A_p} \int_0^{r_p} P_k(r) r dr . \quad (2.2-27)$$

For example, the average plasma DT fusion-power density is given by

$$\frac{P_F}{V_p} = 2.186 \times 10^{-12} g_{DT} n_D n_T \langle \sigma v \rangle_{DT} , \quad (2.2-28)$$

where $\langle \sigma v \rangle_{DT}$ is the fusion reactivity evaluated at the density-weighted volume-averaged temperature, and g_{DT} is the fusion-power profile-correction factor. The values $\langle \sigma v \rangle_{DT}(T_i)$ are obtained using standard fits [26] that have been extended to higher temperature with additional data [27] and have been augmented with Los Alamos experimental measurements and a temperature-dependent fitting function [28] in the range $0 < T_i < 20$ keV.

The ohmic-heating profile-correction factor is

$$g_\Omega = \frac{2\pi}{\eta_{||}(n, T) I_\phi^2 A_p} \int_0^{r_p} \eta_{||} [n(r), T(r)] [j_\phi^2(r) + j_\theta^2(r)] r dr , \quad (2.2-29)$$

where $\eta_{||}$ is the classical Spitzer resistivity, $\propto Z_{eff} T_e^{-3/2}$. For the ARIES-I base case with $T \simeq 20$ keV, the profile enhancement factors are: $g_{DT} = 1.081$, $g_{DD} = 1.327$, $g_{BR} = 1.050$, $g_{CY} = 1.45$, and $g_\Omega = 1.346$.

A 0.10-m scrape-off layer (SOL) at the equatorial plane provides the standoff between the plasma separatrix and the first wall. For ARIES-I, power and particle control is provided by two poloidal-field divertors. A simplified analytic scaling model [29], based on detailed Braams code [30] and other [31] results, has been developed and incorporated into the systems code for a rapid and flexible characterization of the ARIES-I edge-plasma/divertor performance. This model estimates the peak plasma temperature at the divertor plate from

$$T_{PL} = \frac{2m_j (L_s f_d \chi f_r)^2}{k_B (w \gamma W)^2 \lambda^4} , \quad (2.2-30)$$

where,

$m_j \equiv$ plasma ion mass ($2.5 \times 1.66 \times 10^{-27}$ kg),

$L_s \equiv$ is the edge field-line connection length between the watershed and null points,

$f_d \equiv$ fraction of the total thermal power that is deposited on the plate being considered (typically ~ 0.5 for two divertors),

- $\chi \equiv$ cross-field thermal diffusivity in the scrape-off layer (typically $\sim 4 \text{ m}^2/\text{s}$),
- $f_r \equiv$ fraction of the thermal power in the divertor plasma that reaches the plate through the sheath (typically ~ 0.71),
- $w \equiv$ ratio of parallel power flow at the divertor target to that in the scrape-off layer (typically ~ 0.6),
- $\gamma \equiv$ sheath power-flow transmission coefficient (typically ~ 7.2),
- $W \equiv$ ratio of plasma pressure at the divertor target to the pressure at the watershed (typically ~ 0.6), and
- $\lambda \equiv$ radial scale length for the decay of power flow in the SOL appropriate for high-recycle ($T_{PL} \ll T_{SOL}$) or low-recycle limiting cases ($T_{PL} \simeq T_{SOL}$).

The model also estimates the peak divertor-plate heat flux,

$$\hat{q}_{PL} = \frac{P_H (1 - f_{RAD}) f_c f_d f_f \sin \alpha}{2\pi R_T f_x w \lambda}, \quad (2.2-31)$$

where,

$P_H \equiv$ plasma (input) heating power, $P_H = P_\alpha + P_{CD} + P_\Omega$,

$f_c \equiv$ fraction of the thermal power transported into the channel (inboard or outboard) being considered,

$f_f \equiv$ fraction of the power in the divertor plasma that is absorbed by the divertor target (typically ~ 0.9),

$\alpha \equiv$ angle of inclination between the divertor plate and the magnetic surfaces in the poloidal cross section (typically 10°), and

$f_x \equiv$ average flux expansion factor between the SOL and divertor plate (typically 2).

The value of f_{RAD} for a DT plasma at $T \simeq 20 \text{ keV}$ with $Z_{eff} \simeq 1.5$ and a highly reflective ($P_{CY} \simeq 0$) first wall is $\simeq 0.12$. For ARIES-I with an SiC-composite first wall ($R_{CY} \simeq 0.45$), values of $f_{RAD} \simeq 0.5$ are predicted. It should be noted that the above provides only an estimate of T_{PL} and \hat{q}_{PL} . Detailed edge-plasma transport calculations have been performed for ARIES-I (Sec. 5). The estimates given above and detailed calculations both show that T_{PL} and \hat{q}_{PL} decrease as aspect ratio increases, which provides an incentive for high aspect-ratio operation.

The plasma-energy confinement time, τ_E , expressed in terms of the net heating power, $P_{TR} \simeq P_H(1 - f_{RAD})$, is

$$\tau_E = \frac{W_p}{P_H(1 - f_{RAD})}. \quad (2.2-32)$$

The ARIES systems code begins with an input value of the Lawson parameter, $n_i\tau_E$, to establish the physics design point. An internal MacNTAU power-balance calculation [24] and an auxiliary COLIF-code [13] calculation are used to establish the appropriate ion constituent fractions and the corresponding values of $n_i\tau_E$ and τ_E . Once τ_E is known, a comparison can be made to any of a number of proposed empirical scaling relations [5, 16, 32]. It should be emphasized that no particular scaling law is assumed in advance to derive the ARIES-I design point. The value of τ_E for a design point is compared to the various scaling alternatives (*e.g.*, Goldston) by means of a confinement multiplier, $H_j \equiv \tau_E/\tau_E^j$, where the superscript j denotes the particular relation of interest. For example, the Goldston L-mode confinement time is given by

$$\tau_E^G = 3.7 \times 10^{-5} I_\phi R_T^{1.75} a^{-0.37} \kappa_\times^{0.5} \left(\frac{A_i}{1.5}\right)^{0.5} [P_H(1 - f_{RAD})]^{-0.5}, \quad (2.2-33)$$

where A_i is the atomic mass (2.5 for a nominal 50:50 DT fuel mixture).

The current-drive cost and recirculating power have a direct impact on the economics of a steady-state reactor. Therefore, the amount of current drive by external means should be minimized. This is achieved in ARIES-I by maximizing the bootstrap-current contribution and by decreasing the magnitude of I_ϕ (*e.g.*, increased A and q , and decreased β). A solution of the Grad-Shafranov equation that is made self-consistent with both RF-driven and neoclassical current densities [33] provides the following expression

$$\Gamma \equiv \frac{\Delta P_{CD}}{P_{CD}} \simeq \frac{f C \beta_{I_o}}{A^{1/2}}, \quad (2.2-34)$$

where P_{CD} is the current-drive power if all the plasma current has to be driven by external means and ΔP_{CD} is the predicted current-drive power when neoclassical bootstrap effects are included. The on-axis Shafranov poloidal beta is given by

$$\beta_{I_o} = \frac{p_o}{(B_\theta^2/2\mu_o)}, \quad (2.2-35)$$

where B_θ is given by Eq. (2.2-12). The coefficient C is given by

$$C = C_1 - \frac{\alpha_T}{\alpha_p} \left(C_2 + C_3 n_{eo} \frac{T_{io}}{Z_{eff} p_o} \right). \quad (2.2-36)$$

Typically $C_1 = 2.1$, $C_2 = 1.3$, $C_3 = 1.2$, and $f \simeq 0.23$, which in actuality is a weak function of geometry and profiles. Although the expression for Γ was derived for $A \gg 1$, $\kappa = 1$, and $I_{BC}/I_\phi \ll 1$, it agrees well with the numerical result given in Ref. [33]. This model is applied as stated to all ARIES systems calculations and is described in Secs. 2.4.1 and 2.4.2.

Both neutral-beam current drive (NBCD) and ion-cyclotron range-of-frequencies (ICRF) fast-wave current drive (FWCD) were considered for ARIES-I, with lower-hybrid waves being used in both cases to drive current in the edge plasma. The NBCD is a prime candidate for ITER [5] and promises a higher normalized current-drive efficiency,

$$\gamma = \frac{(n_e/10^{20})R_T I_\phi}{P_{CD}}. \quad (2.2-37)$$

The FWCD has a lower unit cost (\$/W), requires less technology extrapolation for RF sources, and is more compatible with the fusion power core (superior maintenance and safety characteristics). Because of these advantages and since no overriding total cost differences were found between NBCD and FWCD, FWCD is selected as the reference current-drive system for the ARIES-I design.

The following expression, corrected for electron trapping effects, is used in the ARIES systems code to scale the normalized efficiency of the FWCD:

$$\gamma = 0.72 \bar{T}_e^{0.77} (0.041 + 0.235 \beta), \quad (2.2-38)$$

where \bar{T}_e is the volume-averaged electron temperature. This expression is based on a fit to 19 self-consistent equilibrium/current-drive calculations with $\alpha_p = 1.4$, $\alpha_n = 1.1$, $Z_{eff} = 1.5$, and volume-averaged ion temperature of $\bar{T} = 12$ keV; limits on $\bar{T}_e > 10$ keV and $\beta \leq 0.08$ are also noted [33].

The tritium-fuel source rate, S_T , in steady state balances the sum of the tritium burnup and loss rate, $L_T = f_t n_i / \tau_p$. The tritium burnup fraction, f_B , is

$$f_B \equiv \frac{S_T - L_T}{S_T} = \left[1 + \frac{1}{g_{DT} f_D \langle \sigma v \rangle_{DT} n_i \tau_E (\tau_p / \tau_E)} \right]^{-1}, \quad (2.2-39)$$

where τ_p , the particle confinement time, is taken to be $\tau_p \approx 4\tau_E$. For the reference ARIES-I design, $f_B \simeq 0.19$. The value of τ_p is assumed to be the same for both fuel ions and the fusion α -particles, resulting in a steady-state concentration, $n_\alpha/n_i \sim 10\%$. The partial pressure, $n_\alpha T_\alpha / (n_i T_i + n_e T_e)$, of the thermalizing α -particles reduces the “useful beta” of the device by $\sim 20\%$, calculated consistent with Ref. [34].

2.2.2. Reactor Engineering Model

The systems-code model for reactor engineering characterizes the first wall, blanket, shield, coils, current-drive, and impurity control hardware in order to provide the basis for the cost estimate of the fusion power core (FPC). Additionally, the reactor power balance is modeled in order to size the balance-of-plant requirements of the ARIES-I electric generating station.

The inboard and outboard thicknesses of the first wall, blanket, and shield are determined by detailed calculations, discussed in Sec. 8, and held fixed by the systems code. The SiC-composite first-wall thickness is 0.012 m on both the inboard and outboard sides of the plasma. The inboard blanket thickness, δ_{Bi} , is 0.67 m, and the outboard blanket thickness, δ_{Bo} , is 0.97 m. The inboard shield thickness, δ_{Si} , is 0.71 m and the outboard shield thickness, δ_{So} , is 0.81 m. Thus, the inboard standoff between the inner plasma edge and the inside face of a TF coil, where the peak toroidal field, $B_{\phi c}$, is found is ~ 1.5 m for all values of a and R_T searched by the systems code.

The toroidal magnetic field is produced by a set of $N_{TF} = 16$ D-shaped TF coils, carrying the coil current, I_c , and producing the on-axis field strength, $B_{\phi}(R_T) \equiv B_{\phi o}$, given by

$$B_{\phi o} = \frac{\mu_o N_{TF} I_c}{2\pi R_T}. \quad (2.2-40)$$

The peak toroidal magnetic-field strength on the inboard leg of the TF coil is given by

$$B_{\phi c} = \frac{\mu_o N_{TF} I_c}{2\pi R_c}, \quad (2.2-41)$$

where R_c is the major radius of the inboard face of the inboard TF-coil leg. Using a convenient model [35] to characterize the poloidal shape of the TF coil, the ARIES-I TF coil is illustrated schematically in Fig. 2.2-1.

The TF-coil set dominates the size and cost of a tokamak reactor, particularly for the ARIES-I design with $B_{\phi c} = 21$ T. The centrum of the TF-coil model is a scaling relationship between the overall current density, $j_{\phi c}$, and $B_{\phi c}$. This TF-coil scaling is given by [36]

$$j_{\phi c} = \frac{0.8 \sigma_{all} - B_{\phi c}^2 / 2\mu_o}{\sigma_{all} (1/j_{SC} + 1/j_{ST}) + (B_{\phi c} R_T / 4) \ln(R_2/R_1) - \sigma_{ST} / j_{ST}}, \quad (2.2-42)$$

where R_1 and R_2 are, respectively, the major radii of the TF-coil inboard and outboard legs, and are in m. The factor $0.8 = 1/1.25$ reflects the typical 25% contribution of insulation and helium-coolant channels to the coil cross section. The allowable stress in the coil

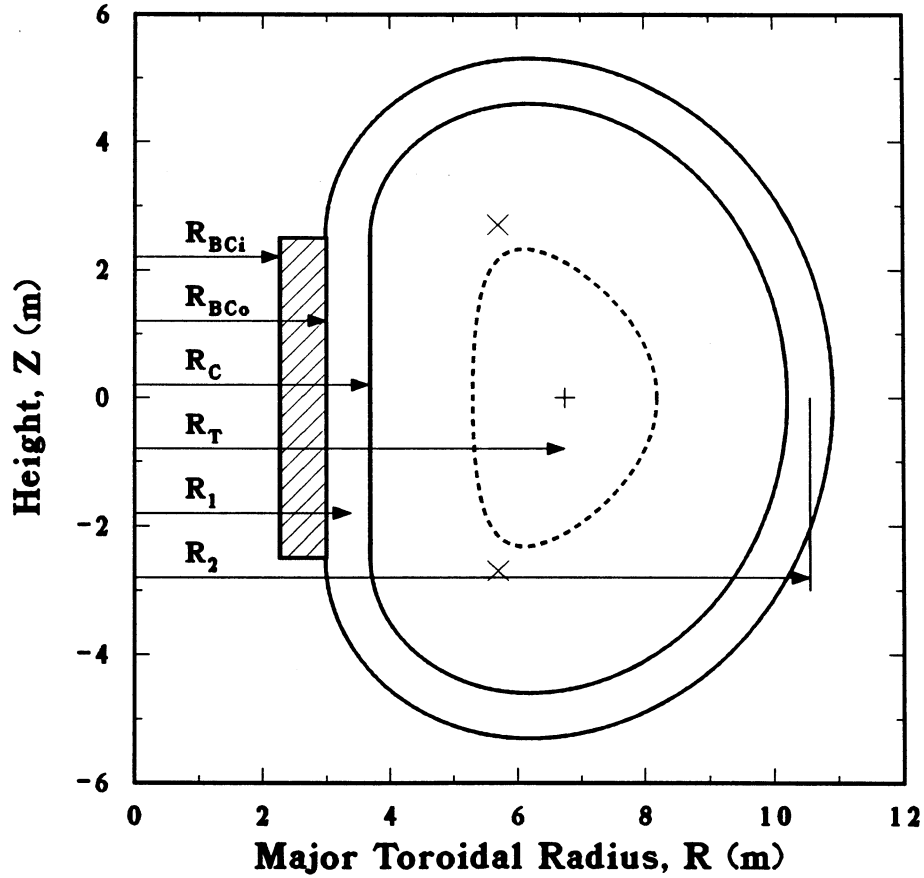


Figure 2.2-1. Schematic elevation view of the ARIES-I plasma and TF coil, showing the bucking cylinder (BC) and the notation used for various major toroidal radii. The view shown is a figure of revolution about the vertical axis ($R = 0$).

support structure is σ_{all} and σ_{ST} is the stabilizer (tensile) yield stress (both in GPa). The stabilizer provides both the usual quench protection and (unlike for ITER) contributes to the overall load-carrying capability. Note that the structural term, $(B_{\phi_0} R_T / 4) \ln(R_2 / R_1)$, dominates except for small values of j_{SC} . This TF-coil scaling relationship is utilized in the ARIES systems code, using the following formula for j_{SC}

$$j_{SC} = 10^4 \frac{1 - (B_{\phi_c} / 46)^2}{B_{\phi_c}^{0.5}}. \quad (2.2-43)$$

Typical for the ARIES-I design is $j_{\phi_c} = 28 \text{ MA/m}^2$ at $B_{\phi_c} = 21 \text{ T}$, compared to the ITER design with $j_c \simeq 14 \text{ MA/m}^2$ at $B_{\phi_c} \simeq 11 \text{ T}$. Figure 2.2-2 gives a typical dependence of j_{ϕ_c} on B_{ϕ_c} for a range of coil scaling assumptions ($R_0 = 7.5 \text{ m}$, $R_1 = 3.5 \text{ m}$, $R_2 = 11 \text{ m}$, $j_{ST} = 200 \text{ MA/m}^2$, and $\sigma_{ST} = 0.8 \text{ GPa}$ for options III and IV).

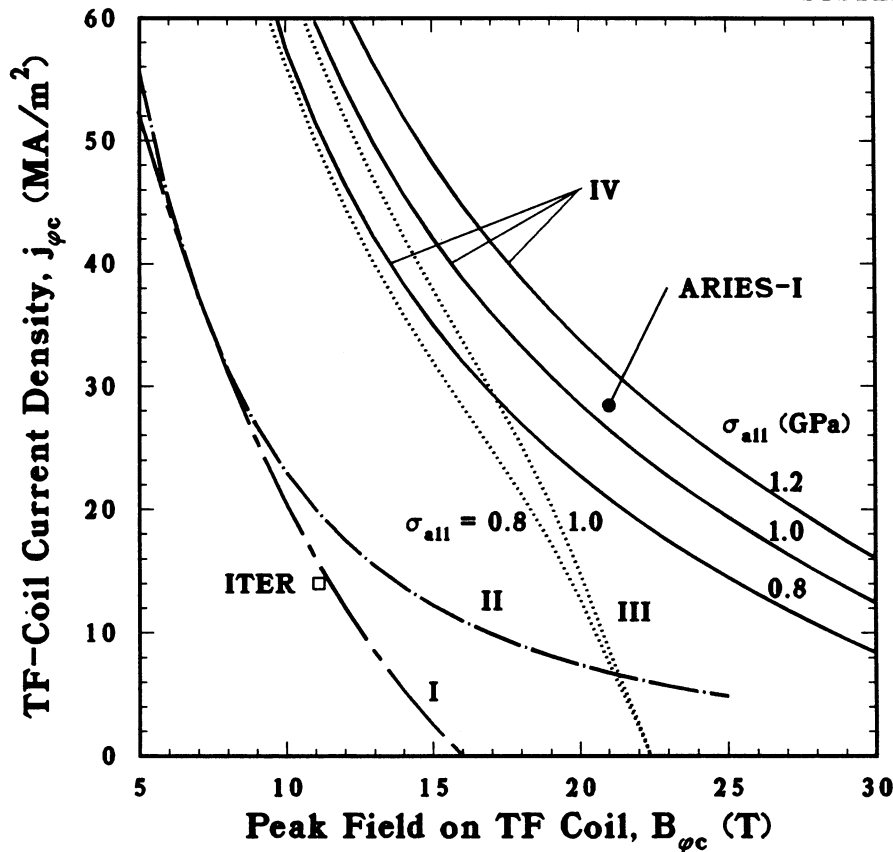


Figure 2.2-2. Scaling relationships for overall TF-coil current density and peak (inboard leg) TF-coil magnetic-field strength. Options I and II (independent of D-coil geometry) were used in the GENEROMAK/ESECOM studies [9, 10, 37, 38]. Options III and IV were developed [36] for advanced high-field applications, consistent with ARIES-I. The ITER design point [5], developed independently of these scaling laws, is shown for comparison.

With the j_c versus B_{ϕ_c} relationship available and N_{TF} specified, the inboard TF-coil cross section can be determined for a given reactor design (*e.g.*, R_T , R_1 , R_2 , B_{ϕ_c} , *etc.*). Specifications of the shield and standoffs determine the vertical half height of the (near-constant-tension) D-shaped TF coil. This D-shaped coil is extended to the outboard leg using the standard shape factor, which, when established by the vertical shield/divertor standoff relative to the elongated plasma, is more than adequate to meet the radial build requirements at the outboard equatorial-plane location. The toroidal-field ripple is monitored at the inboard plasma edge, the plasma magnetic axis, and the outboard plasma edge, with N_{TF} being chosen to hold the outboard plasma-edge ripple to below $\sim 1\%$. The outboard TF-coil “transparency” or coverage factor is also monitored to aid in defining the FPC layout and maintenance.

The net centering forces generated by the TF-coil set are reacted by the hollow bucking cylinder, as is illustrated in Fig. 2.2-1. The critical compressive pressure, P_c , at which the elastic buckling of the (thin) cylinder occurs is approximated by [39]

$$P_c = 0.807 \frac{E \delta_{BC}^2}{h_{BC} R_{BCi}} \left[\left(\frac{1}{1 - \nu^2} \right)^3 \frac{\delta_{BC}^2}{R_{BCi}^2} \right]^{1/4}, \quad (2.2-44)$$

where $E = 2.9 \times 10^{11}$ Pa is Young's modulus for the bucking cylinder material (steel), $\nu \simeq 0.27$ is Poisson's ratio, h_{BC} is the vertical height of the bucking cylinder, and R_{BCi} is the major toroidal inner (bore) radius of the bucking cylinder with thickness, $\delta_{BC} \equiv R_{BCo} - R_{BCi}$. The outer radius of the bucking-cylinder (actually a polygon with $N_{TF} = 16$ sides) coincides with the major radius of the faces of the TF coils at major radius $R_{BCo} = R_1 - \delta_{TF}/2$. The external pressure on the bucking annular cylinder is $P = (R_{BCo}/R_1)(B_{\phi C}^2/2\mu_o) = f_{BC}P_c$, where the factor $f_{BC} = 0.20$ provides a margin of safety. Equation (2.2-44) is solved for the bucking cylinder thickness, δ_{BC} . The bucking cylinder is also monitored for the compressive hoop stress, σ_{θ} , at R_{BCi} , which is approximated by [40]

$$\sigma_{\theta} = - \frac{2R_{BCo}^2 P}{R_{BCo}^2 - R_{BCi}^2}, \quad (2.2-45)$$

which is not allowed to exceed 1.0 GPa. The bucking cylinder is made sufficiently thick to meet the more restrictive of the constraints provided by Eqs. (2.2-44) and (2.2-45). This approximate procedure has been found to be comparable to, but more conservative than, the detailed coil-design calculation reported in Sec. 7. For example, finite-element analysis shows that the peak stress in the ARIES-I TF coil is ~ 700 MPa and, for the same design, the systems code predicts 1.0-GPa stress levels. Additional coil structural support beyond the bucking cylinder must also be provided. Following Ref. [10], the steel structural volume is estimated to be 50% of the TF-coil volume, pending a detailed mechanical design.

The poloidal-field (PF) coils are modeled in the ARIES systems code as two divertor-field (DF) and two equilibrium-field coils. The ratio of DF-coil current to plasma current and the ratio of DF-coil major radius to plasma major radius is calibrated from detailed equilibrium calculations using the NEQ code [41]. These ratios, along with the specification of engineering current density, j_c , in the DF coil allow a coil sizing to be made. Similar PF-coil current and major radius ratios are provided by the NEQ code equilibrium calculations, but a second option using a dipole model to provide the correct vertical field at the plasma outboard edge is adequate for purposes of the systems study.

The ratio of PF-coil to TF-coil mass is monitored to ensure agreement with detailed coil design activities, this ratio typically being in the range of 0.4 to 0.6.

An important design choice in ARIES-I is to locate all PF coils outside the TF-coil set. This specification, along with the requirement that a separatrix be formed within the vacuum chamber in a minimum-energy configuration, gives the dependence of triangularity, δ , on elongation, κ , depicted in Fig. 2.2-3(A); lower κ requires higher δ for a given aspect ratio in order to maintain an *in vacuo* separatrix. The dependence of κ and δ on the inverse aspect ratio, as determined by the NEQ code, is weak and is modeled by [17]

$$\kappa_x = \kappa_o (1 + 0.44 \epsilon^{2.1}), \quad (2.2-46)$$

$$\delta_x = \delta_o (1 + 0.77 \epsilon^3), \quad (2.2-47)$$

where the calibration coefficients are $\kappa_o = 2.1$ and $\delta_o = 0.53$ (*cf.*, Ref. [17]). Maintaining this weak dependence on ϵ but including the δ *versus* κ dependence shown in Fig. 2.2-3 gives [42]

$$\delta_o = -0.5\kappa_o + 1.56. \quad (2.2-48)$$

Since the coupling of PF coils located outside the TF-coil set is poor, and decreases, this δ *versus* κ requirement translates into increased PF-coil currents and mass at the lower values of κ . The required PF-coil mass increase has been estimated by utilizing the multipolar field expansion [42] used to generate Fig. 2.2-3(A) and is expressed in Fig. 2.2-3(B) as follows:

$$\frac{\Delta M}{M_{PF}} = \left(\frac{188}{\kappa_{95}} \right)^{3.0} - 1, \quad (2.2-49)$$

where the reference point has been taken at $\kappa = 1.88$. The dependence on A is weak and, therefore, is not modeled.

The thermal conversion efficiency of the blanket power, P^B , to electricity is denoted by η_{TH}^B . We denote the thermal-conversion efficiency for the divertor-coolant loop by η_{TH}^D , in order to model the case of a compound system (typically $\eta_{TH}^D < \eta_{TH}^B$) or the extreme case where the divertor power, P^D , is dumped to the environment as low-grade (waste) heat ($\eta_{TH}^D \simeq 0$). The power-to-wall area weighted-average thermal-conversion efficiency becomes

$$\eta_{TH} = \frac{P^B \eta_{TH}^B + P^D \eta_{TH}^D}{P^B + P^D}, \quad (2.2-50)$$

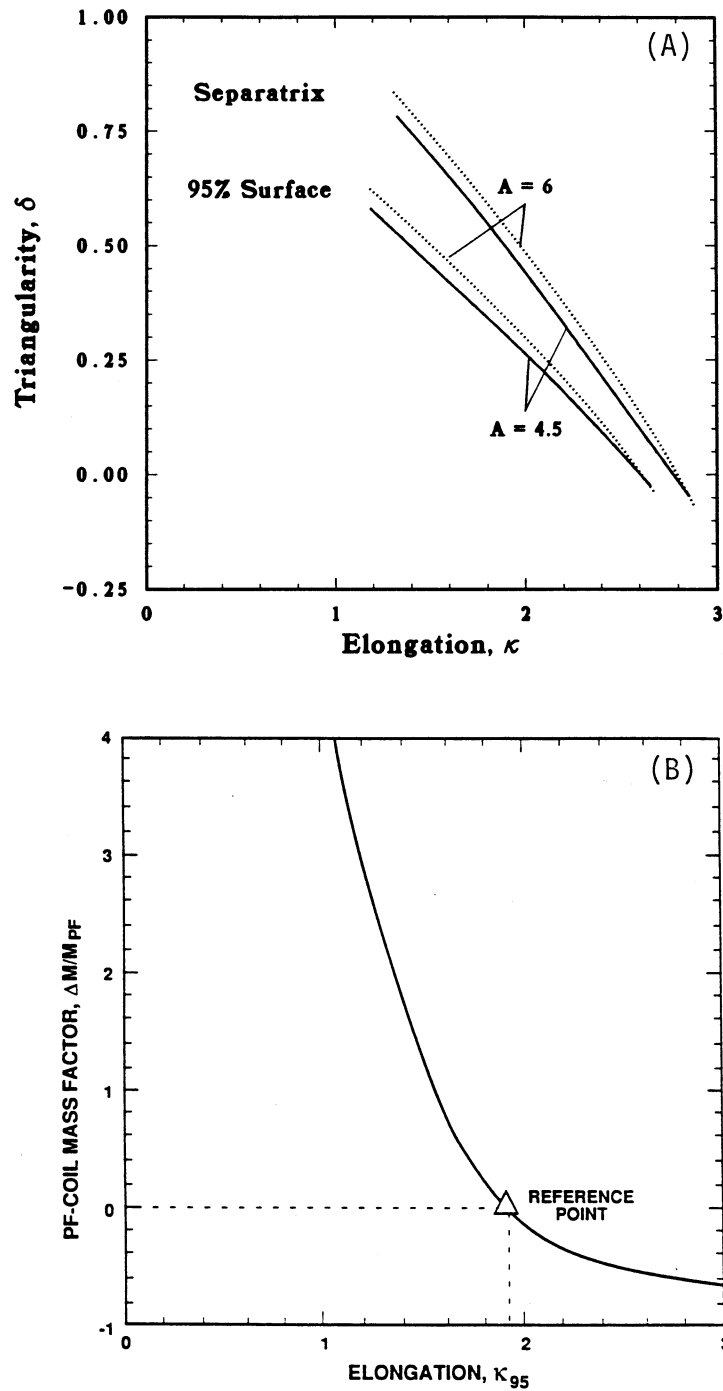


Figure 2.2-3. (A) Plasma triangularity as a function of vertical elongation to ensure a minimum-energy magnetic design for a range of plasma aspect ratios; and (B) Added PF-coil mass required to maintain an *in vacuo* separatrix as the plasma vertical elongation increases.

where

$$P^B = f_{RAD}(1 - f_D)(P_{CP} + P_{CD} + P_{\Omega}) + P_N M_N, \quad (2.2-51)$$

$$P^D = (1 - f_{RAD} + f_{RAD} f_D)(P_{CP} + P_{CD} + P_{\Omega}), \quad (2.2-52)$$

the core plasma-radiation fraction is $f_{RAD} \simeq 0.5$, $f_D = A_D/A_{FW} \simeq 0.25$ is the fraction of the first-wall surface area devoted to the divertor plate surfaces, and $P_{CP} \simeq P_{\alpha}$ is the charged-particle fusion power. The blanket neutron-energy multiplication is $M_N = 1.3$, as found from neutronics calculations reported in Sec. 8. In order to avoid the design complication of two separate coolant circuits, the ARIES-I blanket and divertor use the same helium-coolant inlet/outlet temperatures and pressures to yield $\eta_{TH}^D = \eta_{TH}^B = \eta_{TH} = 0.49$ (Secs. 5, 8, and 9).

The ARIES-I power flow, as modeled in the systems code, is illustrated in Fig. 2.2-4. Given a stipulated target for the net electric-power output, P_E , the thermal-power output, P_{TH} , is determined for a nominal value of the thermal conversion efficiency,

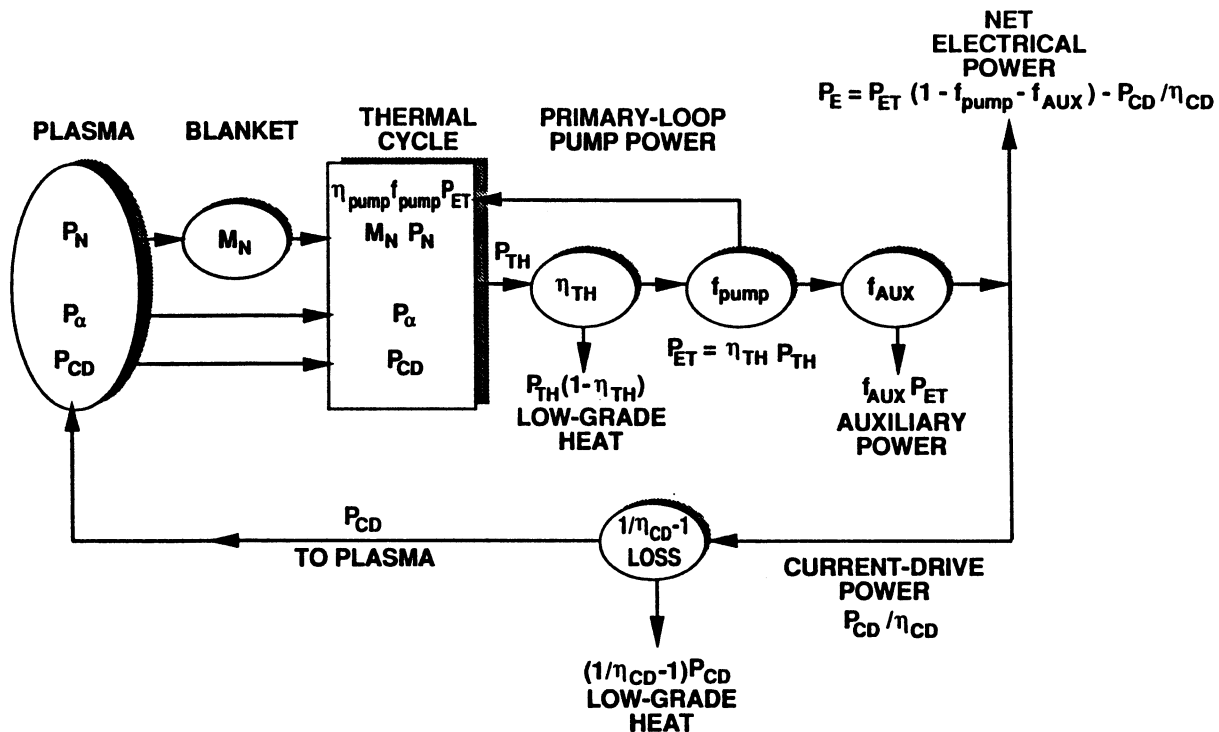


Figure 2.2-4. ARIES-I overall power-flow model as used in the systems code. Typically net electrical power is fixed. Other parameters adjust as plasma radius is varied for fixed plasma aspect ratio.

η_{TH} , such that $P_E = \eta_{TH}(1 - \epsilon)P_{TH}$, where $\epsilon = 1/Q_E$ is the recirculating power fraction and $Q_E \equiv P_{ET}/P_C$ is the engineering Q -value. The gross electric-power output is $P_{ET} = \eta_{TH}P_{TH}$. A fraction f_{AUX} of P_{ET} ($P_{AUX} = f_{AUX}P_{ET}$) is allocated for auxiliary functions. A fraction f_{pump} of P_{ET} ($P_{pump} = f_{pump}P_{ET}$) is allocated for primary-loop pumping power. Of this latter contribution to the recirculating power, it is assumed that $0.90 P_{pump}$ is recoverable as useful thermal power in the primary coolant loop. The engineering Q -value figure of merit, Q_E , can be written as

$$Q_E = \frac{1}{\epsilon} = \eta_{TH} \frac{M_N P_N + P_\alpha + P_\Omega + 0.90 P_{pump}}{P_{AUX} + P_{pump} + (P_{CD}/\eta_{CD})}, \quad (2.2-53)$$

The ratio of fusion power to absorbed current-drive power is the plasma Q -value, or gain, $Q_p \equiv P_F/P_{CD} \simeq 20$ for $Q_E \simeq 5$.

The average 14.1-MeV-neutron first-wall load, $P_N/A_w = I_w$, is given by

$$I_w = \frac{14.06}{17.58} \frac{P_F x}{4\pi^2 A r_p^2}, \quad (2.2-54)$$

where P_F is the DT fusion power and $x \equiv r_p/r_w$ is the plasma filling fraction, which is calculated based on the assumed scrape-off layer thickness, $\delta_s = r_w - r_p = 0.10$ m. Subsequent calculations of the poloidal distribution of the neutron wall load, including the effects of the source distribution, are performed using the NEWLIT code [43]. The peak-neutron wall load as computed from NEWLIT is 3.8 MW/m² at the outboard first wall at the equatorial plane, compared with the average value of 2.5 MW/m².

The total FPC mass, M_{FPC} , is the sum of coil, blanket, shield, and structure component masses. The ratio P_E/M_{FPC} in units of kWe/tonne is used as the FPC mass power density (MPD) figure of merit. The threshold of marginal economic interest, met by ARIES-I, has been identified at ~ 100 kWe/tonne [44]. Higher power-density systems lead to higher values of MPD, with the MPD value that minimizes COE being highly dependent on the confinement concept.

2.3. COSTING AND ECONOMICS

The plasma physics and reactor engineering models of the ARIES systems code together provide a characterization of the ARIES-I FPC that is adequate for conceptual cost projections. The systems-code unit-cost data base is summarized in Table 2.3-I. Unit costs for NBCD and FWCD options are summarized in Table 2.3-II.

Table 2.3-I.
Fusion-Power-Core Unit Costs (1988 \$)^(a)

Material/Component	Mass Density (kg/m ³)	Unit Cost (\$/kg)
Breeder materials		
Li (natural)	500	47.5
Li ₂ O	2,000	47.5
LiAlO ₂	2,550	47.5
Li ₄ SiO ₄	2,400	47.5
Li ₂ ZrO ₃	4,150	51.3 ^(b)
FLiBe	2,000	74.3 ^(c)
PbLi	9,400	4.3
Structural materials		
PCA	7,800	52.8
RAF	7,800	52.8
Fe-1422	7,800	21.1
HT-9/Cu	7,800	58.1
SiC (composite)	3,200	400.0
Al	2,700	14.2
Other materials		
SiC (bulk)	3,200	50.0
Be	1,850	530.5
BeO	3,000	212.0
Cu	8,900	58.5
C	2,000	10.7
B ₄ C	2,500	21.2
Coils		
Ternary Nb ₃ Sn	7,300	90.0
Nb ₃ Sn	7,300	80.0 ^(d)
NbTi	7,300	70.0
Cu	7,300	57.0
Divertor system	—	63.0 k\$/m ²

^(a)Reported 1986-\$ unit costs (Ref. [10], primary source) are updated to 1988 \$.

^(b)Ref. [45].

^(c)~\$50/kg suggested [46].

^(d)Ref. [47].

Table 2.3-II.
Current-Drive Unit Costs (1988 \$)

	System Efficiency, η_{CD}	Unit Cost (\$/W)
2-MeV neutral beam	0.68	3.0
Lower hybrid (80 MHz)	0.68	1.25
ICRF fast-wave ^(a)		
80 MHz	0.84	1.0
158 MHz	0.72	1.0
250 MHz	0.65	2.0
800 MHz	0.63	2.0
2500 MHz	0.48	2.0
8000 MHz	0.44	2.5

^(a)Ref. [48]

The estimated cost of electricity (COE, mill/kWh) is the most important evaluation tool for optimizing and comparing with alternative energy sources. The estimated COE is the object function of the parametric systems analysis (PSA) code. Both constant-1988 and then-current-1994 dollar analyses (consistent with the assumed $\tau_c = 6$ -y construction time) are used to evaluate the ARIES-I costs. The bus-bar energy cost is given by

$$\text{COE} = \frac{C_{AC} + (C_{O\&M} + C_{SCR} + C_F)(1 + y)^Y}{8760 P_E p_f}, \quad (2.3-1)$$

where

COE = Cost of electricity in constant or then-current dollars (mill/kWh);

C_{AC} = Annual capital cost charge, equals the "overnight" total capital cost multiplied by the fixed charge rate;

C_i = Cost of account i ;

$C_{O\&M}$ = Annual operations and maintenance cost, $C_{40} + C_{41} + \dots + C_{47}$;

C_{SCR} = Annual scheduled component-replacement cost, $C_{50} + C_{51}$;

C_F = Annual fuel costs, C_{02} and C_{03} ;

y = Annual escalation rate;

Y = Construction period (year);

P_E = Net plant electric-power output (MWe);

p_f = Plant availability factor;

TDC = Total direct cost = $\sum_{i=20}^{26} C_i$;

C_{IDC} = Interest during construction, $C_{97} = f_{IDC}$ TDC;

C_{EDC} = Escalation during construction, $C_{98} = f_{EDC}$ TDC;

TCC = Total capital cost = $\sum_{i=20}^{98} C_i$.

The detailed methodology for calculating the time-related cost factors is described in Refs. [9] and [49] and will not be repeated here. This description differs from the U.S. fusion-reactor-community standards [50, 51] used in the period 1980 to 1985 because of a slightly different "s-shaped" spending profile assumed, but represents the pending standard for U.S. fusion-reactor studies for the foreseeable future [52]. Levelized annual fixed-charge-rate (LAFCR) values are summarized in Table 2.3-III. The reference TITAN study [2] assumed an annual inflation/escalation rate, $y = 0.06/y$, to give, under the standard assumptions [49], an annual utility cost of money (COM) of $x = 0.09/y$, a constant-dollar-mode LAFCR of $0.08/y$, and a corresponding then-current-dollar-mode LAFCR of $0.136/y$. Factors used to obtain interest-during-construction and escalation-during-construction costs are summarized in Table 2.3-IV. The TITAN study used the upper set of factors ($y = 0.06/y$ and $x = 0.09/y$). The lower set, assuming $y = 0.05/y$ and $x = 0.10/y$, is characteristic of the older U.S. fusion-community standard [49, 53]. Differences between the standards, however, are not large. The economic parameters assumed in the costing model used in the ARIES-I study are summarized in Table 2.3-V.

The direct-cost account entries, C_i , are obtained by applying relevant (installed) unit-cost estimates (*e.g.*, $\$/W$, $\$/kg$, $\$/m^3$), where known, to the calculated usage of these items in the conceptual design, such that $C_i(\$) = u_i(\$/\text{unit})X_i$ (unit). A learning curve or mass production credit is taken for a "tenth-of-a-kind" commercial reactor installation,

Table 2.3-III.
Effective Cost of Money (COM) and
Levelized Annual Fixed-Charge Rate (LAFCR)^(a)

Escalation Rate, y (%/y)	COM, x (%/y)	LAFCR (%/y)
0	4.2	8.0 ^(b) (10.0) ^(c,d)
2	5.8	9.7
4	7.4	11.6
5	NA	NA (15.0) ^(d)
6 ^(b,e)	9.0 ^(b,e)	13.6 ^(e) (16.5) ^(c)
8	10.6	15.8
10	12.2	18.1

^(a)Ref. [49].

^(b)TITAN study [2] reference case for constant-dollar mode.

^(c)Ref. [9].

^(d)Ref. [50].

^(e)TITAN study [2] reference case for then-current-dollar mode.

consistent with U.S. fusion-reactor design-community practice. The ARIES-I study, like STARFIRE [54] and most other U.S. fusion-reactor designs reported in the last decade, assumes unit costs consistent with these learning curve [55] credits, rather than first-of-a-kind unit costs (including R&D) appropriate for ITER [5] or some other reported designs [8]. A “75% learning curve” (*i.e.*, 0.75 progress ratio, p), as used for ARIES [47], represents the expectation that each doubling of production represents a $(1 - p)$ reduction in unit costs. A “tenth-of-a-kind” reactor represents, nominally, ~ 3.3 doublings of production or $\sim 50\%$ cost reduction relative to initial costs. Of course, actual production experience varies [55].

Table 2.3-IV.
Time-Related Cost Factors^(a)
as Functions of Construction Lead Time

Lead Time, Y (y)	Capitalization Factors,		Interest Factor,
	f'_{cap} (nominal dollar)	f'_{cap0} (constant dollar)	f'_{IDC}
<u>For $y = 0.06/y$ and $x = 0.09/y$^(b)</u>			
1	0.0788	0.0177	0.0556
2	0.1558	0.0287	0.0908
3	0.2386	0.0399	0.1274
4	0.3273	0.0513	0.1652
5	0.4224	0.0629	0.2042
6 ^(c)	0.5244	0.0747	0.2444
7	0.6338	0.0866	0.2858
8	0.7511	0.0986	0.3284
9	0.8768	0.1109	0.3723
10	1.0117	0.1233	0.4176
<u>For $y = 0.05/y$ and $x = 0.10/y$</u>			
1	0.0812	0.0297	0.0617
2	0.1558	0.0484	0.1011
3	0.2359	0.0676	0.1424
4	0.3217	0.0873	0.1853
5	0.4135	0.1076	0.2299
6	0.5120 ^(d)	0.1282 ^(d)	0.2761 ^(d)
7	0.6174	0.1494	0.3240
8	0.7303	0.1711	0.3738
9	0.8512	0.1933	0.4254
10	0.9808	0.2161	0.4790

^(a) $f_j \equiv 1 + f'_j$.

^(b) *cf.*, Ref. [9], Table D.I, p. 237.

^(c) TITAN study [2] base case for $Y = 6$ y construction time.

^(d) *cf.*, Ref. [50]; (IDC and EDC are, respectively, interest and escalation during construction.)

$f'_{cap} \equiv (f_{IDC} + f_{EDC}) = (0.316 + 0.190) = 0.506$, $f'_{cap0} = 0.129$, $f'_{IDC} = 0.316$.

Table 2.3-V.
Reference ARIES-I Economic Parameters^(a)

Plant life (y)	30
Plant lead time (y)	6
Indirect cost factor	0.35
Contingency factor	0.10
Factor for escalation and interest during construction	1.1652
Nominal capacity factor	76%
Spare parts multipliers	
Blanket	1.0
Coil	1.0
Limiter	1.0
Effective cost of money	
Nominal dollars	0.0957
Constant dollars	0.0435
Inflation rate (y^{-1})	5%
Effective tax rate	0.3664
Tax depreciation life (y)	
Overall plant	15
Replaceable blankets, <i>etc.</i>	5
Fixed charge rate	
Nominal dollars	0.1638
Constant dollars	0.0966

^(a) *cf.*, Ref. [10], Table 3.1.

Often, the cost data base consists of cost scaling relationships of the form

$$C_j (\$) = c_j (X_j)^{e_j}, \quad (2.3-2)$$

where X can be either a descriptive variable (*e.g.*, power, mass, volume) or a scaled variable, X_j/X_{REF} , related to a reference value, X_{REF} of X_j , and e_j is an appropriate scaling exponent (usually $0 < e_j < 1$). Equation (2.3-2) can be rewritten in the form

$$C_j = \frac{c_j (X_j)^{1-e_j} (X_j)^{e_j}}{(X_j)^{1-e_j}} = \left[\frac{c_j}{(X_j)^{1-e_j}} \right] X_j, \quad (2.3-3)$$

which allows the definition of a (variable) unit cost

$$u_j = \frac{c_j}{(X_j)^{1-e_j}}, \quad (2.3-4)$$

and is a dependent function of the descriptive variable, X_j , itself. While the cost accounting scheme allows for detailed cost breakdowns (to four levels), only a relatively sparse, but comprehensive, subset of items are estimated and reported explicitly. The cost scaling exponents, e_j , used in the ARIES-I study are typically consistent with those of the U.S. fission nuclear-reactor experience [56] and represent the inclusion of quality-control costs associated with nuclear-grade (N-stamped) components. Potential cost savings derived from the substitution of conventional (non-nuclear) components under the condition of demonstrable inherent safety are significant but controversial [57]. Two sets of such cost factors are summarized in Table 2.3-VI. These savings can amount up to 25% on selected items, but have not been included in the ARIES-I data base. The essential elements of the ARIES-I cost data base are summarized in Table 2.3-VII. Costs that date from sources using a 1980-dollar reporting base are scaled to a 1988 reporting base by using the multiplicative factor 1.424.

For purposes of costing in the systems code, the reactor building is divided into a variable-volume reactor cell (housing the FPC and vacuum tank) and a fixed-volume region (housing the primary heat-transport loops). The volume of the latter portion is estimated to be $1.55 \times 10^5 \text{ m}^3$ and is similar to that of STARFIRE [54] after escalating costs. The reactor room is modeled as a rectilinear enclosure extending horizontally 9 m beyond the FPC with a height approximately three times that of the FPC, such that $V_{RB} (\text{m}^3) = 16 (R_T + r_s + 9)^2 (6r_s) + 1.55 \times 10^5$. The basic building structure (Acct. No. 21.2.1) is priced at $\$300/\text{m}^3$, a value between that of STARFIRE [54] and MARS [60] designs. To this value is added 2 M\$ for building services (Acct. No. 21.2.2), $\$40 \text{ M}$ for containment structures (Acct. No. 21.2.3), and $\$10.1 \text{ M}$ for architectural costs

(Acct. No. 21.2.4). The ARIES FPC is represented by most of the reactor equipment (Acct. No. 22.1) items.

The reactor-torus replacement-cost estimate applies a factor of 2 to the direct cost of these components to allow for the handling and replacement of the spent reactor-torus modules. For an assumed first-wall fluence life, $I_w\tau = 20 \text{ MWy/m}^2$ at a cost-optimized neutron wall loading of $I_w \simeq 2.5 \text{ MW/m}^2$ and a plant factor $p_f \simeq 0.76$, routine FPC replacement occurs every six years. Account No. 50 represents $\sim 9\%$ of the base-case COE for ARIES-I and is distinct from the nominal annual operations and maintenance

Table 2.3-VI.
Safety-Assurance Cost-Credit Factors^(a)

Cost Area	Perkins' Factor [10, 57]	ICF Factor [10, 58]
Blankets	2.0	1.11
Shield	2.0	1.11
Coils	1.44	1.11
Reactor building and hot cells	1.47	4.0
Other structures and improvements	1.47	1.15
Heat transfer and transport	2.5	1.11
Other reactor plant equipment	1.0	1.11
Turbine plant equipment	1.0	1.18
Electrical plant equipment	1.75	1.54
Miscellaneous plant equipment	1.3	1.67
Heat reject system	1.25	1.11
Land	1.0	1.18
Indirect costs	1.25	1.32
O&M costs	1.0	1.32
All other cost areas	1.0	1.0

^(a)Divisor factor applied to cost model accounts.

Table 2.3-VII.
Summary of ARIES-I/TITAN Cost Data Base^(a,b)

Acct. No.	Account Title	Cost (M\$, 1980 ^(c))
20.	Land and Land Rights	3.3
21.	Structures and Site Facilities	
21.1	Site improvements and facilities	11.28
21.2	Reactor building	$3.0 \times 10^{-4} V_{RB} + 39.5$
21.3	Turbine building	33.5
21.4	Cooling structures	$7.135 (P_{ET}/1000)^{0.3}$
21.5	Power supply and energy storage bldg.	9.16
21.6	Miscellaneous buildings	76.5
21.7	Ventilation stack	1.81
22.	Reactor Plant Equipment (RPE)	
22.1	Reactor equipment	
22.1.1.1	Breeding material:	Table 2.3-I
	Liquid metal (LM): PbLi ^(d,e)	(see Acct. No. 26.1)
	Li ^(d,f)	(see Acct. No. 26.1)
	Water solution: LiNO ₃ ^(d,g)	$(7.83 f_{6Li} + 2.46) \times 10^{-3} M$
22.1.1.2	Blanket and first-wall structure	$0.0533 M_{BL}$
22.1.1.3	Be multiplier ^(g)	$0.3338 M_{Be}$
22.1.2	Shield:	
	V alloy ^(f)	$0.1855 M_{SHD}$
	Ferritic steel ^(g)	$0.0157 M_{SHD}$
22.1.3	Magnet coils:	
	Normal conducting	Table 2.3-I
	Superconducting	Table 2.3-I
22.1.4	Supplemental (RF) heating systems	Table 2.3-II
22.1.5	Primary structure and support	$0.1125 V_{STR}$
22.1.6	Reactor vacuum system	$0.015 M_{VAC}^{(f)} + 2.5 \text{ (kg/d)}$

Table 2.3-VII (Cont'd)

Acct. No.	Account Title	Cost (M\$, 1980 ^(c))
22.1.7	Power supply (switching, energy storage):	
	Normal-conducting coils	18.55 \$/kVA
	Superconducting coils	296.7 \$(kVA) ^{0.8}
	IBC ^(f)	37.09 \$/kVA
	OFCD ^(f,g)	37.09 \$/kVA
	Other	1.0
	TF IBC busbars ^(f)	3.034
	DF IBC busbars ^(f)	1.625
22.1.8	Impurity control system	0.66 A_D
22.1.9	Direct energy conversion ^(h)	0.0
22.1.10	ECRH breakdown system	1.589
22.2	Main heat-transfer system	
22.2.1	Primary coolant:	
	Li ^(f)	$u_j = 0.2013 [P_{TH}(1 - f_w)]^{-0.2}$ (i) $X_j = P_{TH}(1 - f_w)$
	He, H ₂ O ^(g)	$u_j = 0.1030 [P_{TH}(1 - f_w)]^{-0.2}$ (i) $X_j = P_{TH}(1 - f_w)$
22.2.2	Intermediate coolant system	$u_j = 0.1030 P_{TH}^{-0.2}$ (i) $X_j = P_{TH}$
22.2.3	Secondary coolant system	$u_j = 0.1030 (P_{TH} f_w)^{-0.2}$ (j,e) $X_j = P_{TH} f_w$
22.3	Auxiliary cooling systems	$6.7 \times 10^{-4} P_{TH}$
22.4	Radioactive waste treatment	$1.2 \times 10^{-3} P_{TH}$
22.5	Fuel handling and storage	
22.5.1	Pellet injectors	3.709 M\$ each $\times 2$ (f,g,i)
22.5.2	Fuel processing system	0.5 (g/d) ^{0.7}
22.5.3	Fuel storage	3.709
22.5.4	Atmospheric tritium recovery	0.2 (m ³ /h) ^{0.6}
22.5.5	Water detritiation system:	
	TITAN-I, ARIES-I	5
	TITAN-II	140

Table 2.3-VII (Cont'd)

Acct. No.	Account Title	Cost (M\$, 1980 ^(c))
22.6	Other reactor plant equipment	$1.09 \times 10^{-3} P_{TH}$
22.7	Instrumentation and control	23.41
23.	Turbine Plant Equipment	
23.1	Turbine generators	$59.9 (P_{ET}/1000)^{0.7}$
23.2	Main steam system	$4.80 (P_{TH}/2860)$
23.3	Heat rejection systems	$0.0632 (P_{TH} - P_{ET})^{0.8}$
23.4	Condensing system	$13.8 (P_{ET}/1000)^{0.9}$
23.5	Feed heating system	$7.55 (P_{TH}/2860)$
23.6	Other turbine plant equipment	$40.9 (P_{ET}/1000)^{0.6}$
23.7	Instrumentation and control	$7.8 (P_{ET}/1000)^{0.3}$
24.	Electric Plant Equipment	
24.1	Switchgear	$8.6 (P_{ET}/1000)$
24.2	Station service equipment	$14.2 (P_{ET}/1000)$
24.3	Switchboards	$5.4 (P_{ET}/1000)$
24.4	Protective equipment	2.11
24.5	Electrical structures and wiring containers	$11.12 + 6.28 (P_{ET}/1440)$
24.6	Power and control wiring	$23.0 + 13.0 (P_{ET}/1440)$
24.7	Electrical lighting	8.2
25.	Miscellaneous Plant Equipment	
25.1	Transportation and lifting equipment	15.68
25.2	Air and water service systems	12.35
25.3	Communications equipment	6.22
25.4	Furnishings and fixtures	1.20
26.	Special Materials	
26.1	Reactor LM coolant/breeder: ^(d)	
	PbLi ^(e)	$(7.83 f_{6Li} + 2.46) \times 10^{-3} M_{LM}$
	Li ^(f)	$(1169 f_{6Li} + 58.0) \times 10^{-3} M_{LM}$
26.4	Other	0.25
26.5	Reactor-building cover gas (Argon) ^(f,h)	0.13

Table 2.3-VII (Cont'd)

Acct. No.	Account Title	Cost (M\$, 1980 ^(c))
90.	Total Direct Cost (TDC)	
91.	Construction Services and Equipment (10% of TDC)	
92.	Home Office Engineering and Services (10% of TDC)	
93.	Field Office Engineering and Services (10% of TDC)	
94.	Owner's Cost (5% of TDC)	
95.	Process Contingency (5% of TDC) ^(h)	
96.	Project Contingency (10% of TDC)	
97.	Interest during Construction (IDC)	
98.	Escalation during Construction (EDC)	
99.	Total Capital Cost (TCC)	

^(a)Gross electric power, P_{ET} , net electric power, P_E , and total thermal power, P_{TH} , are given in MW. Volumetric, V , (m^3) or corresponding mass, M , (tonne) unit costs for the FPC and related items are given as follows:

Reactor building, $V_{RB} = 4(R_T + r_s + 9)^2(6r_s) + 1.55 \times 10^5$ (m^3);

Blanket structure (5%), M_{BL} (tonne); Shield, M_{SHD} (tonne);

Magnet coils, M_C (tonne); Structure, V_{STR} (m^3);

Vacuum tank, $M_{VAC} = (0.07)(7.8)2\pi[(R_T + r_s + 3)^2 + 4r_s(R + r_s + 3)]$ (tonne);

Divertor-plate surface area, A_{DIV} (m^2).

^(b)See Ref. [2] for detailed TITAN design cost summaries.

^(c)1980 costs are multiplied by 1.424 to yield 1988 costs.

^(d)Liquid metal, M_{LM} (tonne): ${}^6\text{Li}$ enriched, $0.075 < f_{{}^6\text{Li}} < 0.90$ [59].

^(e)Applicable to CRFPR.

^(f)Applicable to TITAN-I.

^(g)Applicable to TITAN-II.

^(h)Not applicable to ARIES-I.

⁽ⁱ⁾cf., Eq. (2.3-4).

charge (Acct. Nos. 40–47, 51), previously estimated [50, 53] to be $\sim 2\%$ of the direct cost, or scaled by [61]

$$C_{OP} (\text{M}\$/\text{y}) = 69.2 (P_E/1200)^{0.5} \quad (2.3-5)$$

for the ARIES study.

Some historical drift in the financial parameters used to estimate the indirect, interest, and contingency costs are summarized in Table 2.3-VIII. This drift complicates making cost comparisons between published fusion-reactor results if adjustments for differing assumptions are not made. Updates reflect, for example, changes in U.S. tax rates [56, 62]. Comparisons with competitive fossil and fission energy sources are facilitated by a common set of modern financial guidelines.

Table 2.3-VIII.
Evolution of Financial Parameters

Reference	(a)	(b)	(c)	(d)	(e)
Fixed charge rate (constant dollars)	0.10	0.10	0.08	0.0844	0.0966
Fixed charge rate (then-current dollars)	0.15	0.15	0.136	–	0.1638
Inflation/cost escalation rate (y^{-1})	0.05	–	0.06	0.06	0.05
Effective cost of money (y^{-1})	0.05	–	0.042	0.09	0.0605
Interest during construction ^(f)	0.1290	0.1303	0.1124	–	0.1652
Indirect costs (\times TDC)	0.35	0.23	0.35	0.375	0.35
Project contingency costs (\times TDC)	0.0	0.0	0.10	0.20	0.10

^(a)Ref. [53].

^(b)STARFIRE [54].

^(c)TITAN [2, 49].

^(d)ESECOM/GENEROMAK [10, 37].

^(e)ARIES-I [62].

^(f)Design and construction lead time, $\tau_c = 6$ y.

2.4. DESIGN POINT DETERMINATION

2.4.1. Safety Factor Variation: Beta vs Magnetic Field

Based on considerable theoretical and experimental effort in recent years, confidence has increased that tokamaks may be operated continuously with the equilibrium toroidal current, I_ϕ , generated by RF waves [63]. Furthermore, recent studies have indicated that RF current drive is marginally acceptable for a commercial reactor [64] in agreement with earlier estimates [65]. Emphasis is placed now on improving the performance of large, current-driven tokamaks. The effort in the current-drive theory has been generally aimed at maximizing the local ratio of driven parallel current density to absorbed RF power, j_{\parallel}/p_{RF} . A more relevant parameter for a reactor is the plasma Q_p (ratio of the fusion power, P_F , to the absorbed RF power, P_{RF}). Recent work [66] has shown that the RF current-drive power can be lowered by adjusting the MHD equilibrium in order to maximize the bootstrap-current contribution. This work departs from previous studies in two respects: (1) the RF current drive is calculated self-consistently for specified equilibria that have been explicitly shown to be stable and (2) MHD equilibrium is chosen to optimize the bootstrap-current contribution while retaining stability.

One way of modifying the MHD equilibrium to reduce the current-drive power would be simply to reduce I_ϕ for a fixed toroidal beta, $\beta \equiv 2\mu_0 p/B_\phi^2$ (B_ϕ is the vacuum magnetic field at the major radius, R_T ; and p is the volume-averaged pressure). However, the theoretical and experimental efforts [20] in the past decade have shown that the minimum ratio of current to beta is limited to

$$\frac{I_\phi}{\beta} = R_T B_\phi (A C_T), \quad (2.4-1)$$

where A is the aspect ratio, and the Troyon coefficient, C_T , is on the order of 0.03 T m/MA. It should be noted that theoretical MHD studies predict a "second stability" region [67] as the poloidal beta increases, in which case I_ϕ can be reduced below the limit of Eq. (2.4-1). Here, poloidal beta is taken to be $\beta_I \equiv 2\mu_0 p/(\mu_0 I_\phi A/2\pi R_T S)^2$, where $S \equiv c/(2\pi a)$, a is the plasma minor circumference, and $a = R_T/A$. Because of a lack of experimental data for second stability with high β , this regime of operation was ruled out for the ARIES-I design.

The alternative approach is to simultaneously reduce I_ϕ and β while keeping the I_ϕ/β ratio fixed at the value given by Eq. (2.4-1) and holding the plasma pressure constant. This can be done by increasing q_0 , the safety factor at the magnetic axis, which is, in fact, another way of increasing β_I . As q_0 increases, the bootstrap contribution to the current

increases and can exceed 80% even for the relatively flat density and pressure profiles that might characterize a reactor. Even though raising q_o in an ohmically driven device is difficult, because the current tends to peak sharply in the center where the temperature and conductivity are highest, increased q_o is feasible in an RF-driven device. Several non-inductive current-drive experiments [68–70] have, in fact, demonstrated this ability to modify the safety factor. In addition, more experimental evidence that shows that bootstrap currents do contribute substantially to the total current at high values of β_I is becoming available [69, 71–73].

A disadvantage of this approach is that the magnetic field must increase as β decreases in order to keep the plasma pressure and fusion power constant. However, the reductions in current-drive power can be dramatic because a smaller amount of current needs to be driven. The relative costs of magnetic field and current drive for a particular device determine the attractiveness of this option. Indications exist that the trade-off is favorable as long as the field is not too large [74].

In order to illustrate these points, equilibria were compared for tokamak reactors having the same P_F and the same physical dimensions. The pressure, temperature, density, and impurity content were all held constant when comparing equilibria and calculating the current-drive requirements. Holding the plasma pressure constant implies that this set of equilibria satisfy

$$\beta B_\phi^2 = K^2, \quad (2.4-2)$$

where K is constant.

Several degrees of freedom are left in the equilibrium calculation, and parameters had to be chosen carefully in order to achieve MHD stability. A simple, broad pressure profile, $p(\tilde{\psi}) = p_o \tilde{\psi}^\alpha$, where $\tilde{\psi}$ is the normalized poloidal-flux function, was used with $\alpha = 1.4$. The diamagnetism was specified as $RB \equiv F(\tilde{\psi}) = R_o B_o (1 - \delta \tilde{\psi}^{\alpha_F})^{1/2}$. These choices give conventional, peaked, current profiles and ensure that the current density vanishes at the limiter boundary ($\tilde{\psi} = 0$). The peak pressure, p_o , is determined by P_F , and the parameters δ and α_F were chosen to produce a series of equilibria for each value of q_o . The edge safety factor, q , was adjusted from a low value until ideal $n = 1$ stability (with the conducting wall far from the plasma) and $n \rightarrow \infty$ ballooning stability were both achieved. The kink stability was calculated using the PEST-2 code [75], and the ballooning stability was calculated with the Phillips ballooning code [76]. These equilibria were constrained to satisfy Eq. (2.4-1) with $C_T = 0.030$ T m/MA, as expected for highly elongated plasma cross sections [76].

The three equilibria with parameters given in Table 2.4-I were chosen as representative of the issues involved and are near the limit for $n = 1$ kink stability. The case with $q_o = 2.07$ was found to be stable to $n = 1.5, 2,$ and 3 toroidal modes as well. The equilibrium with $q_o = 1.07$ was in the first stability regime for ballooning, but near the limit (shown in Fig. 2.4-1). For the other two equilibria, the unstable region between the first and second stability regimes (Fig. 2.4-1) has shrunk to zero, so a stable access to higher β exists for these cases with regard to ballooning modes. All three equilibria are

Table 2.4-I.
MHD Parameters and Current-Drive Requirements
of Three Representative Equilibria^(a)

q_a	1.07	1.60	2.07
q_b	3.56	6.24	8.47
I_o (MA)	11.3	8.81	7.58
β (%)	3.23	1.98	1.51
B_o (T)	10.5	13.4	15.3
β_I	2.00	3.27	4.40
P_{RF} (MW)	348.	269.	233.
γ (10^{20} MA/MW-m ²)	0.34	0.38	0.37
P_{RF}^B (MW)	223.	97.7	46.8
γ^B (10^{20} MA/MW-m ²)	0.59	1.05	1.99
$Q^B \equiv P_F/P_{RF}^B$	11.	24.	50.

^(a)For equilibria stable to $n = 1$ kink and $n \rightarrow \infty$ ballooning modes. Values with a superscript B include the bootstrap contribution. All cases having $R_o = 6.0$ m, $A = 6.0$, elongation = 2.25, $S = 1.69$, $C_T = 0.30$ T m/MA, and the same plasma parameters: $\bar{n}_e = 1.9 \times 10^{20}$ m⁻³, $n_{eo} = 2.7 \times 10^{20}$ m⁻³, $\bar{T}_e = 16$ keV, $T_{eo} = 42$ keV, and $Z_{eff} = 1.5$, resulting in $P_F = 2360$ MW with DT fuel.

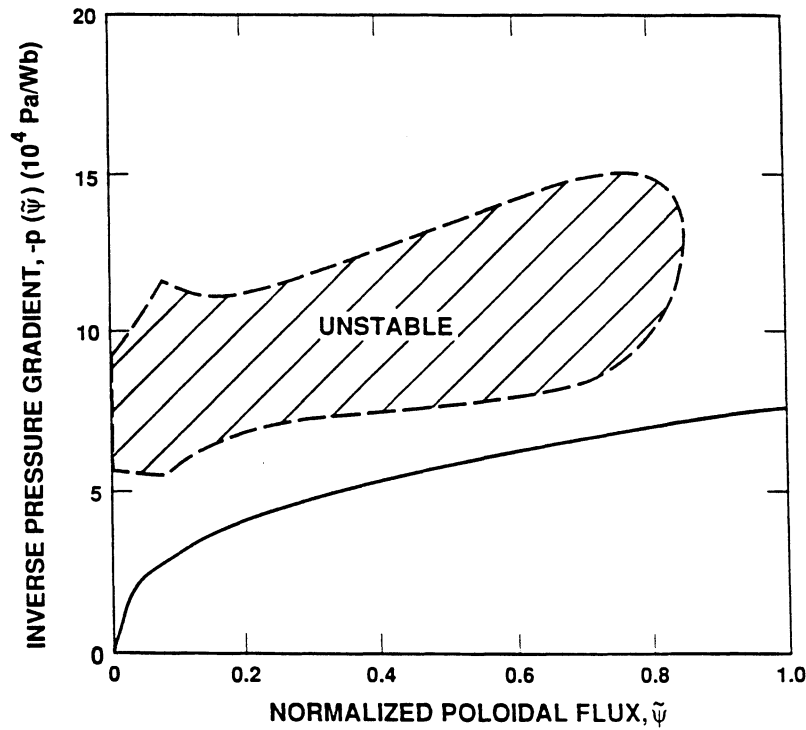


Figure 2.4-1. Phillips diagram [76] for the case $q_o = 1.07$. The ballooning-unstable region for each flux surface in the plasma is predicted (shaded). As long as $-p'(\tilde{\psi})$ is below this region, the equilibrium is stable in the first stability regime. The second stability regime is above this region. No ballooning-unstable regions were found for the other two cases shown in Table 2.4-I.

robust in the sense that nearby equilibria with similar values of the safety factor are also stable for the value of C_T assumed. However, the $n = 1$ kink instability can arise when q is in a narrow range around an integer [76]; this result underscores the desirability of carefully controlling the safety factor with the RF current drive.

The existence of MHD equilibria with desirable stability properties was established and checked to determine whether they could be created with RF current drive. Simulations based on experimentally calibrated transport models [77] suggest that density profiles may be rather flat in a reactor. Electron densities of the form $n_e(\tilde{\psi}) = n_{e0}\tilde{\psi}^{\alpha_n}$ and temperature profiles of the form $T_e(\tilde{\psi}) = T_{e0}\tilde{\psi}^{\alpha_T}$ were used with $\alpha_n = 0.3$ and $\alpha_T = 1.1$. The RF current drive was provided by two different waves: (1) the lower-hybrid slow wave at 8.0 GHz, which suffers strong Landau damping and thus generates current only near the plasma edge and (2) the fast wave, which is known to couple well to electrons at

high density and temperature [78–80] and can provide the current density in the plasma interior.

Following the method of Ref. [64], a set of rays was selected for each equilibrium and the required RF power in each ray was calculated; a least-squares fit to $G(\tilde{\psi}) \equiv \langle j_{\parallel} B \rangle / \langle B^2 \rangle$ from the equilibrium was made in order to duplicate the cases in Table 2.4-I. Seven rays were used for these calculations, which were able to match the important equilibrium quantities such as the current density and safety factor to about 5% or better; additional rays would give a closer match at the expense of more computer time. The current drive was calculated with and without the bootstrap contribution, and the results are summarized in Table 2.4-I. When the bootstrap contribution is not included, P_{RF} decreases modestly in proportion to I_{ϕ} as q_o increases. This trend is expected from the relationship

$$P_{RF} = \frac{n_e R_T I_{\phi}}{\gamma}, \quad (2.4-3)$$

where previous work [64] has shown that γ is a function only of \bar{T}_e and Z_{eff} .

The full benefit of the high safety factor is evident when the bootstrap current is included [33]. As shown on Fig. 2.4-2, the bootstrap contribution to $G(\tilde{\psi})$ for the case $q_o = 1.60$, is a substantial portion of the total current requirement. The RF-driven currents only need to supply the remaining fraction of the total, thereby greatly reducing the RF power requirements. The large decrease of bootstrap-aided current-drive power, P_{RF}^B , as $q(o)$ increases is shown in Table 2.4-I and in Fig. 2.4-3. This decrease may be explained heuristically by rewriting P_{RF} from Eq. (2.4-3) along with Eqs. (2.4-1) and (2.4-2) as $P_{RF} = n_e R_T^2 K \sqrt{\beta} / (A C_T \gamma)$. This formula shows the benefit of increasing C_T or reducing β and can be modified to display the influence of the bootstrap effect by expressing β in terms of β_I and by defining $\Gamma \equiv 1 - (\gamma/\gamma^B) = 1 - (P_{RF}^B/P_{RF})$ as the bootstrap “fraction” of the total current. The result is

$$P_{RF}^B = \frac{5 \times 10^6 (\bar{n}_e R_T^2 S K) (1 - \Gamma)}{A \gamma \sqrt{\beta_I}}. \quad (2.4-4)$$

Since the bootstrap current remains constant for fixed density and temperature profiles, Q increases as the required equilibrium current, I_{ϕ} , decreases. The dependence of Q_p as a function of β_I is plotted in Fig. 2.4-3. Calculations [33] with $q_o \approx 1.1$ (Fig. 2.4-3) have previously quantified the monotonic increase of Q_p with β_I . Based on Eq. (2.4-4), the high β_I values associated with a high safety factor lead to large reductions in P_{RF}^B . It can be seen that $\Gamma \geq 0.8$ can be achieved even with rather flat density profiles, given a sufficiently large safety factor. This result can lead to tokamak reactors with $Q_p \approx 25 - 50$ compared to $Q_p \approx 7 - 15$ [64] without the bootstrap contribution.

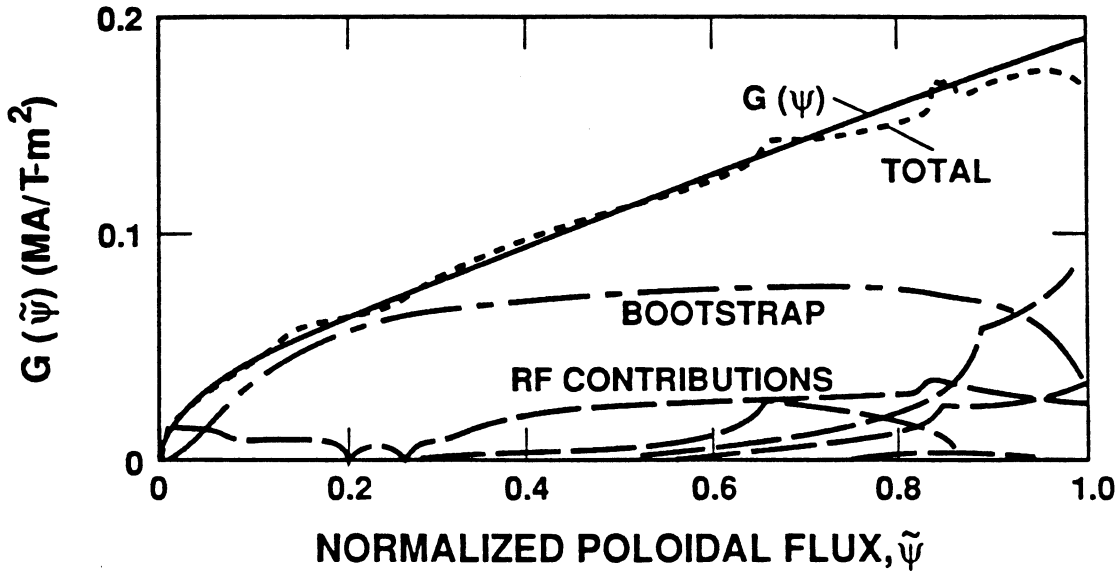


Figure 2.4-2. Contributions to the current density for the case $q_0 = 1.60$. The solid line is the required $G(\tilde{\psi}) \equiv \langle j_{\parallel} B \rangle / \langle B^2 \rangle$ for the specified equilibrium. The chain-dashed curve is the bootstrap contribution, and the other curves are the contributions for each of the RF waves. The dotted curve is the total, which matches the required $G(\tilde{\psi})$. This example had 16 MW of slow waves with $\eta_{\parallel} = 1.5 - 3.2$ and 82 MW of fast waves with $\eta_{\parallel} \approx 1.2$.

In conclusion, specified MHD equilibria with desirable stability properties were reproduced numerically by launching properly tailored RF power spectra. With RF current drive, it is not necessary to constrain the safety factor to profiles typical of ohmic current drive ($q_0 \approx 1.0$). Increasing the safety factor while maintaining stability can provide large bootstrap contributions to the current, even assuming flat density profiles. This approach greatly reduces the current-drive requirements. A possible drawback is that the toroidal field would have to increase to maintain the same fusion power for a reactor.

2.4.2. Temperature Variation: Current-Drive Power vs Fusion Power

Key issues in optimizing steady-state tokamak-reactor design concern the variation of fusion power and current-drive power with the plasma temperature. In order to quantify the trade-offs, it was necessary to know the dependence of the normalized current-drive efficiency, γ , on plasma temperature. The values of $\gamma(\bar{T}_e)$ and $\gamma^B(\bar{T}_e)$ are calculated

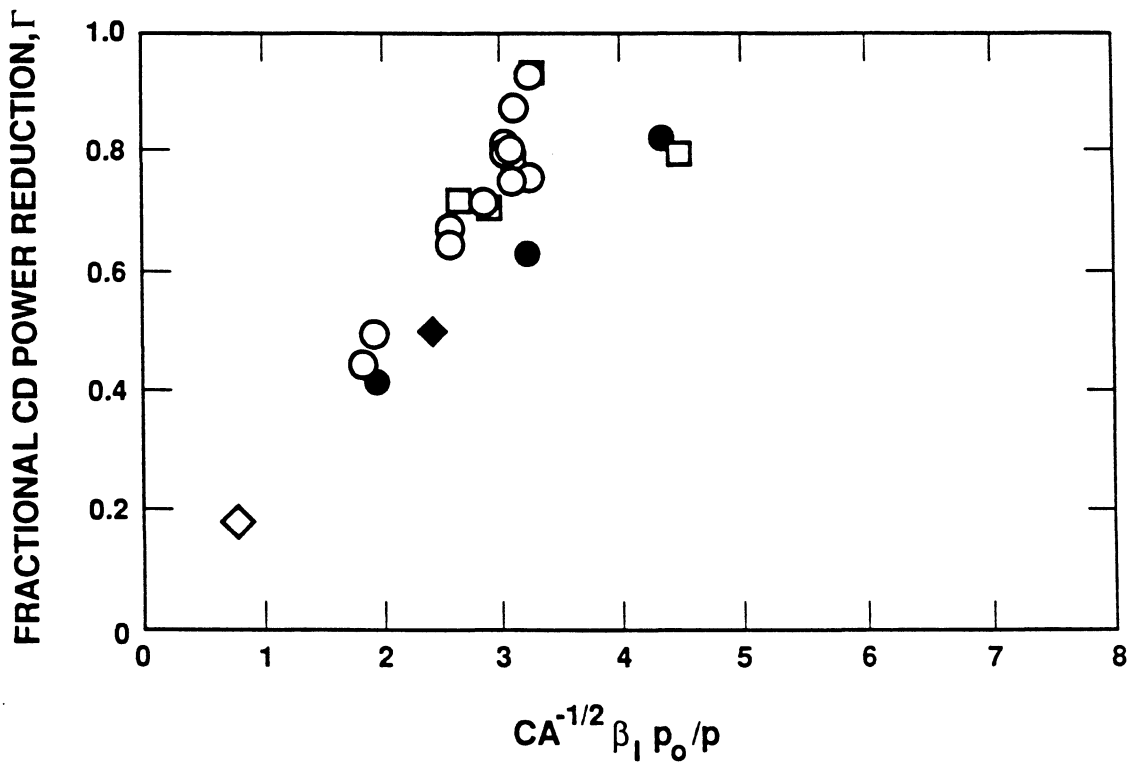


Figure 2.4-3. Fractional RF current-drive-power reduction resulting from the bootstrap effect as a function of β_I (normalized). Parameter C is a function of the plasma profiles. Open symbols are former results for $q_o \approx 1.1$. Solid symbols are new results for equilibria tested for MHD stability and correspond to flat density profiles with $\alpha_n = 0.3$. Solid circles correspond to equilibria in Table 2.4-I and the solid diamond is an additional case for $A = 4.7$, $\kappa = 1.6$, and $q_a = 1.4$.

with self-consistent fast-wave currents and 2-D MHD equilibria (superscript B indicates quantities in the presence of bootstrap currents).

The RF current-drive model described in Sec. 4.4 includes magnetic trapping effects and also includes the Alfvén-wave-type damping associated with low-frequency ion-cyclotron range-of-frequency (ICRF) fast waves. Also, the bootstrap current is calculated with the best available model, as is described in Sec. 4.3. These new results are thus more accurate than previous estimates of γ and γ^B [33, 64]. The geometry is the reference ARIES-I: $R_T = 7.245$ m, $a = 1.555$ m (95% flux surface), $\kappa = 1.6$, $\delta = 0.5$. The equilibrium is also the reference: pressure, $\beta = 1.9\%$; axis safety factor, $q_o \approx 1.3$; and $Z_{eff} = 1.6$, with a broad density and narrow temperature profile (Sec. 3.5).

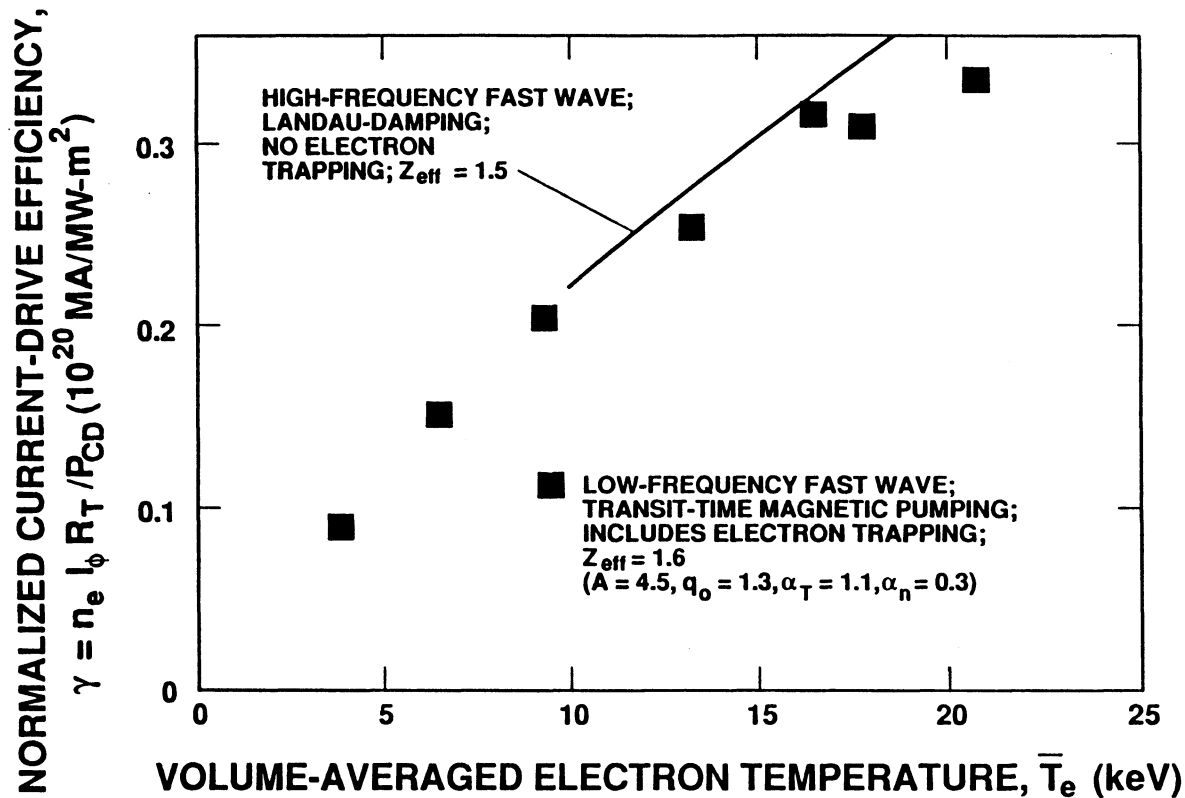


Figure 2.4-4. Calculated normalized current-drive efficiency (points) in the absence of any bootstrap effect, including electron trapping for low-frequency fast waves with transit-time-magnetic pumping, for ARIES-I. The solid curve is the prediction of earlier theory [64].

The first task in this study was to calculate the power balance, plasma density, and fusion power for a range of temperatures ($\bar{T}_e = 4 - 22$ keV) with a fixed magnetic field ($B_\phi = 11.6$ T), and plasma current ($I_\phi = 11.0$ MA). Confinement times were adjusted such that $T_i \approx T_e$, the α -particle density was set at 10% of the fuel ions, and oxygen content was adjusted so $Z_{eff} = 1.6$. In addition, the electron confinement time was adjusted until the auxiliary heating power was roughly consistent with the current-drive power. For fixed beta and magnetic field, the fusion power density peaks at $\bar{T}_i \approx \bar{T}_e \approx 6$ keV [7]. However, the electron density is very high at low temperatures ($n_e = 5 \times 10^{20} \text{ m}^{-3}$ at 6 keV), which presents a problem for noninductive current drive.

The second step in this study, therefore, made an explicit calculation of γ and γ^B at several points over the temperature range. An additional penalty to the high density

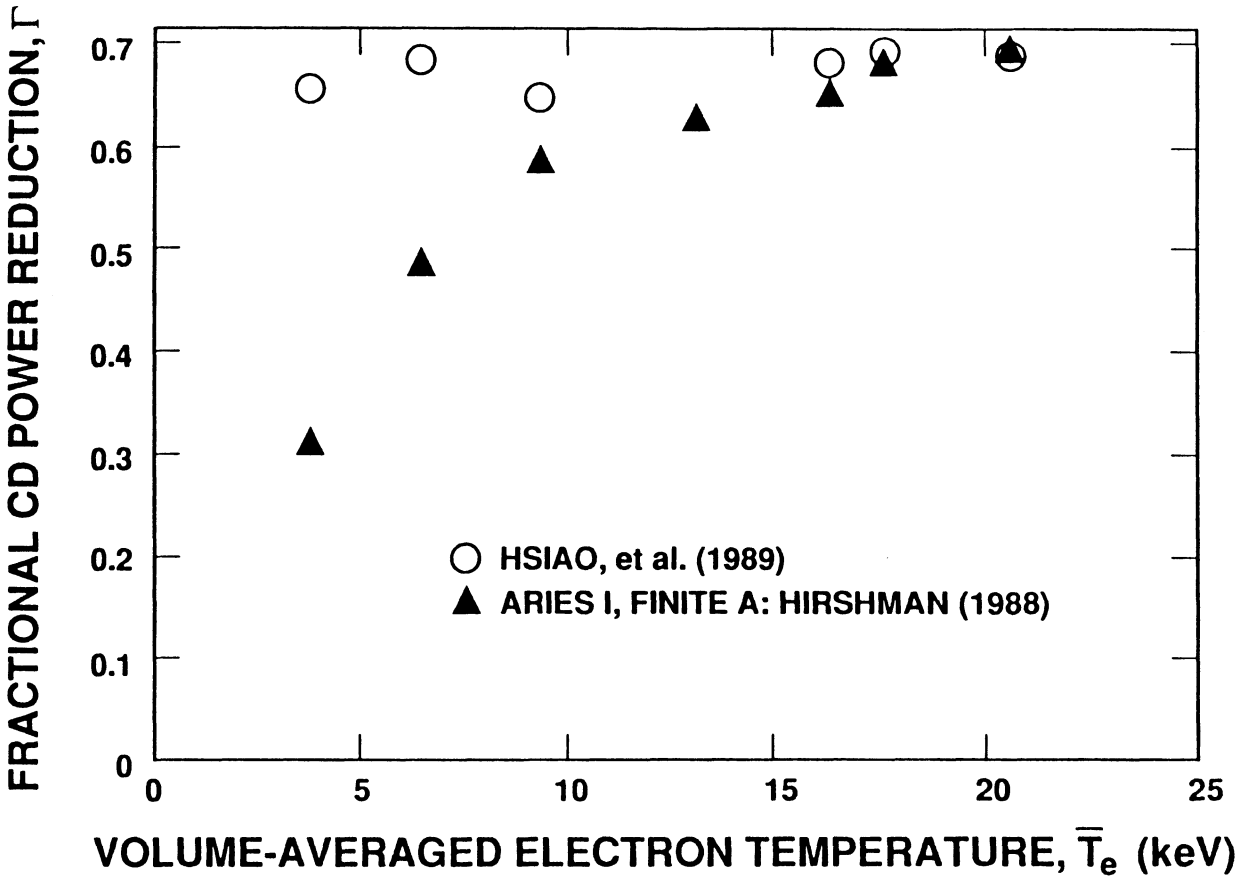


Figure 2.4-5. Fractional current-drive-power reduction due to the bootstrap effect. Triangles are present calculations with finite aspect-ratio theory [81]; circles are predictions of previous work [33] but assuming banana regime (high- T_e) operation.

operation at low temperature is the inherent dependence of q on \bar{T}_e . Results are shown in Fig. 2.4-4 as discrete points and are compared with the simple scaling of $\gamma(\bar{T}_e)$ previously developed [64]. Whereas the Alfvén-wave/transit-time magnetic-pumping current-drive mechanism raises q relative to the Landau damping mechanism, the electron-trapping effect reduces q relative to the simple field result. These effects tend to offset each other, with the fortunate result that the simpler scaling of $\gamma(\bar{T}_e)$ is an acceptable approximation to the improved calculation.

The same series of equilibria were generated with the bootstrap current included. The fractional reduction in current-drive power, Γ , resulting from bootstrap effects [81] is plotted in Fig. 2.4-5; this result is compared with the previous predictions [33]. At all temperatures \bar{T}_e above 15 keV, both calculations agree ($\Gamma \simeq 0.65$) and depend only on profiles and poloidal beta and, to a smaller extent, on Z_{eff} and aspect ratio. The

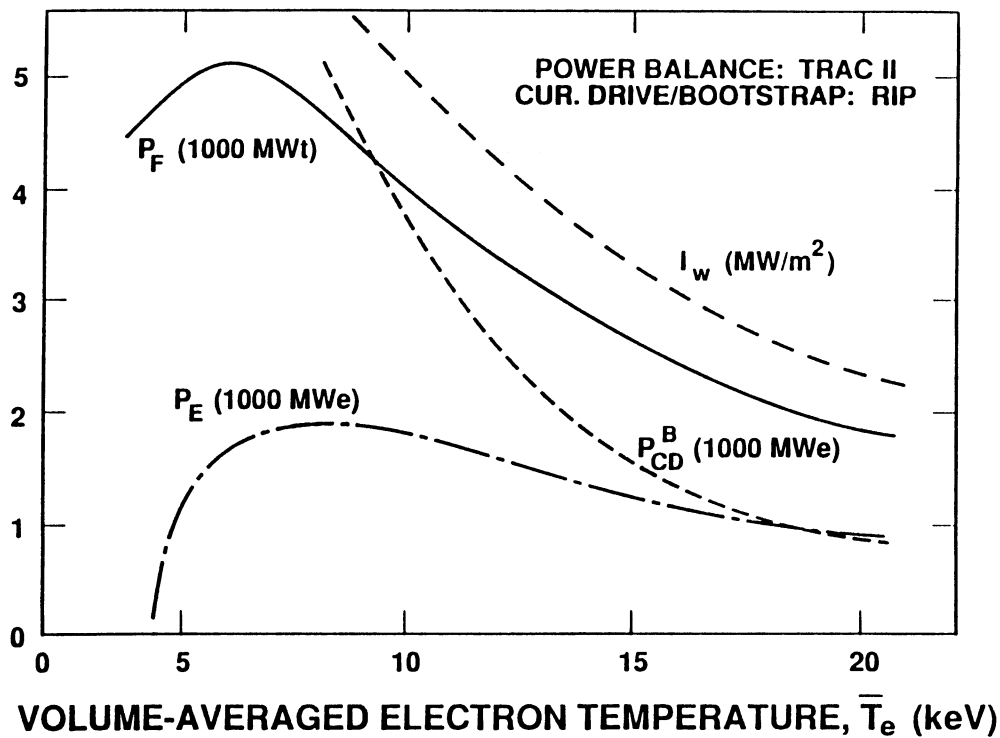


Figure 2.4-6. Plasma performance and current-drive power at different temperatures for ARIES-I ($R_T = 7.3$ m, $B_\phi = 11.6$ T, $\beta = 0.019$, $I_\phi = 11.0$ MA, and $Z_{eff} = 1.6$). Plotted are fusion power, P_F ; average 14-MeV-neutron wall load, I_w ; bootstrap-aided current-drive power, P_{CD}^B ; and net electric power, P_E .

calculations show, however, a sharp decrease in Q_p as the temperature is reduced below ~ 10 keV. This decrease results from increased collisionality since the bootstrap-current coefficients diminish as more of the plasma enters the plateau regime.

Using the above results for the current-drive efficiency and the bootstrap fraction, Fig. 2.4-6 shows the plasma performance and current-drive power as function of the plasma temperature. The bootstrap-aided current-drive power, P_{CD}^B , is modest at the reference ARIES-I temperature (~ 100 MW) but grows quickly as \bar{T}_e is reduced (~ 1000 MW at 6 keV). Hence, the circulating power fraction is minimized at high temperature [82] ($Q_p \equiv P_F/P_{CD}^B \geq 20$ at $\bar{T}_e = 18$ keV, while $Q_p \leq 10$ at $\bar{T}_e = 10$ keV). However, the net electric power is at a maximum at the lower temperature, $\bar{T}_e \leq 10$ keV, using parameters similar to those of the final ARIES-I design: current-drive system efficiency, $\eta_{CD} = 0.71$, blanket neutron-energy multiplication, $M_N = 1.28$, and thermal conversion efficiency,

$\eta_{TH} = 0.47$. There are additional engineering penalties associated with low temperature operation, specifically a high neutron wall load ($I_w > 4 \text{ MW/m}^2$) and high heat load on the divertor (α -particle power plus large current-drive power). In fact, the STARFIRE study demonstrated [54, 82] that the minimum cost of power will occur at some intermediate temperature between the maxima in P_E and Q_p . The reference temperature for ARIES-I ($\bar{T} \simeq 17 \text{ keV}$) also reflects this trade-off.

2.4.3. Parametric Results

The results of Secs. 2.4.1 and 2.4.2 establish the plasma engineering basis of the ARIES-I design point on a self-consistent modeling framework. Using interim ARIES-I parameters, an extensive parametric survey was performed and summarized in Ref. [74]. General trends of this analysis also remain valid for the reference ARIES-I design. At that point in the ARIES-I study, an advanced $\text{Nb}_3(\text{Al}, \text{Ge})$ TF-coil conductor with a 46-T critical field was under consideration, leading to a design point with $B_{\phi c} = 24 \text{ T}$ at $A = 4.5$. The advanced $\text{Nb}_3(\text{Al}, \text{Ge})$ superconductor is presently available only in the form of tape conductors. Losses in the tape conductor were found to be large during a disruption such that the TF coils would probably quench. Therefore, subsequent effort in the ARIES study has considered using a ternary Nb_3Sn TF-coil conductor with an ~ 26 -T critical field, leading to a design point with $B_{\phi c} = 21 \text{ T}$, again at $A = 4.5$.

Generally speaking the cost of the tokamak reactor (for any A) increases as its size increases (*i.e.*, larger a or R_T with fixed A). Small values of a are associated with higher values of $B_{\phi o}$ and $B_{\phi c}$, resulting in a thicker build of the TF-coil inboard leg and a thicker bucking cylinder. Low values of A yield higher values of β and reduced B_{ϕ} . The correspondingly higher values of I_{ϕ} result in higher P_{CD} and, together with a lower bootstrap-current fraction ($f_{BC} = I_{BC}/I_{\phi}$), yield lower values of Q_E . Higher values of $B_{\phi c}$ at higher A are associated with a more massive coil set and lower MPD values. The costs of more massive coils at higher A trade off with the dominant costs of current drive at low A to minimize the COE near $A \simeq 4.5$. The trade-off between FPC cost, reflected in MPD, and recirculating power costs associated with current drive, reflected in Q_E , is a recurrent theme in optimizing the tokamak reactor that, for the unit costs assumed, generally favors high MPD at the expense of reduced Q_E for a given A . Low values of Q_E also result in increased thermal-cycle and electric-power-generation costs, not in the FPC itself, but in the balance of plant.

Economies of scale [83, 84] built into the cost model (Sec. 2.3) suggest some incentive for larger plant sizes (*e.g.*, 1200 MWe *cf.*, STARFIRE [54]). Conversely, economic

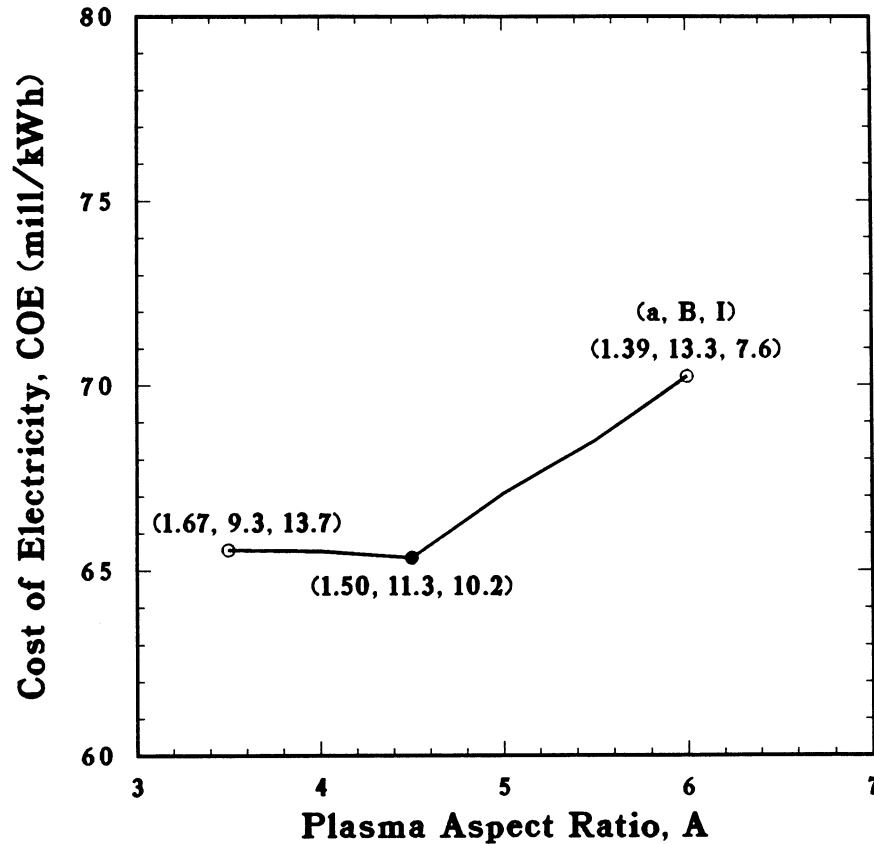


Figure 2.4-7. Projected COE as a function of plasma aspect ratio. The net plant output is fixed at $P_E = 1000$ MWe, peak TF-coil field at $B_{\phi c} = 21$ T, and TF-coil allowable stress at $\sigma_{all} = 1000$ MPa. The COE exhibits a shallow minimum (~ 65 mill/kWh) for $A \simeq 4.5$. The ARIES-I design point is denoted by the filled circle.

considerations of utility “coverage ratios” and other technical considerations (*e.g.*, divertor performance) suggest smaller plant sizes. A nominal value of $P_E = 1000$ MWe was selected for ARIES-I similar to TITAN-I [2] (actually ~ 970 MWe).

Figure 2.4-7 displays the ARIES-I projected COE as a function of aspect ratio, A , for a fixed net electric power output, $P_E = 1000$ MWe. The peak TF-coil allowable stress is $\sigma_{all} = 1000$ MPa. Mass power density (MPD) is typically lower at higher A as the required higher toroidal field leads to more massive TF-coils at lower $j_{\phi c}$ (MA/m²) and the engineering Q -value is higher, reflecting lower current-drive power as plasma current decreases. Divertor-plate plasma temperature and peak heat flux are monotonically lower as A increases. Average neutron wall load increases as A increases. The COE exhibits a shallow minimum near ~ 65 mill/kWh for $A = 4.5$.

The sensitivity of the ARIES-I design point to plasma and plasma engineering assumptions and technological performance were also investigated (Fig. 2.4-8 through 2.4-11). Figure 2.4-8(A) displays the COE as a function of the Troyon coefficient, C_T ($\beta \propto C_T$). It may be possible to increase C_T for fixed aspect ratio, A , and safety factor, q , by optimizing and controlling the plasma profiles. The bootstrap-current fraction, f_{BC} , and current-drive efficiency, γ , are fixed at the reference values. The peak field on the TF coil is also fixed at its nominal value, $B_{\phi c} = 21$ T. Lower values of C_T (*i.e.*, lower β) result in higher COE values. The gain to be obtained from higher C_T values is significant, but less pronounced. Figure 2.4-8(B) plots projected COE as a function of FWCD wall-plug efficiency, η_{CD} . As η_{CD} increases, there is a direct reduction in the cost of current-drive power as well as less-obvious cost reduction in the overall thermal cycle as Q_E increases. However, the leverage on COE available to incremental changes in η_{CD} is fairly modest because the ARIES-I overall design approach has been successful in reducing the plasma current by operating at high A , by increasing the bootstrap fraction, and by using high magnetic field. For the reference ARIES-I design, the current-drive cost is \sim \$100 M and plasma Q -value is 20.

Figure 2.4-9(A) illustrates the interaction of peak field on the TF coil, $B_{\phi c}$, and MPD. The MPD increases as a function of $B_{\phi c}$ from \sim 60 kWe/tonne at 13 T to \sim 100 kWe/tonne at $B_{\phi c} \simeq 21$ T, representative of the ARIES-I design point. Access to higher fields using more advanced conductors or structures than invoked for ARIES-I would continue this improvement. Of course, increased MPD is not an end in itself and improvements in MPD are limited by the peak heat load and other constraints. Rather, increased MPD is used as a predictor of improved COE performance [38, 44], as indicated in Fig. 2.4-9(B). The COE decreases as a function of increasing MPD values for ARIES-I as well as for many other fusion reactor concepts. Finally, displaying the same information in Fig. 2.4-10, the COE is plotted as a function of $B_{\phi c}$.

The impact of MPD on the direct cost of major components of the ARIES-I is shown in Fig. 2.4-11. Consistent with Fig. 2.4-9, MPD increases as peak TF-coil field increases and the FPC size (mass) decreases for fixed $A = 4.5$. The magnet cost, dominated by the TF-coil set, remains unchanged. First wall, blanket, and shield costs do drop for smaller reactors at higher MPD. The current-drive and main heat-transport costs are decoupled from MPD to first order. The cost contribution of reactor equipment (Acct. No. 22.1) to reactor plant equipment (Acct. No. 22) is \sim 74%. The ratio of reactor plant equipment to total direct cost is RPE/TDC \simeq 63%. Total direct cost (Acct. No. 90) is projected to be \sim \$2.1 B (1988) and the total capital cost (Acct. No. 99) is \sim \$3.6 B, for a “tenth-of-a-kind” plant, including future learning-curve cost credits.

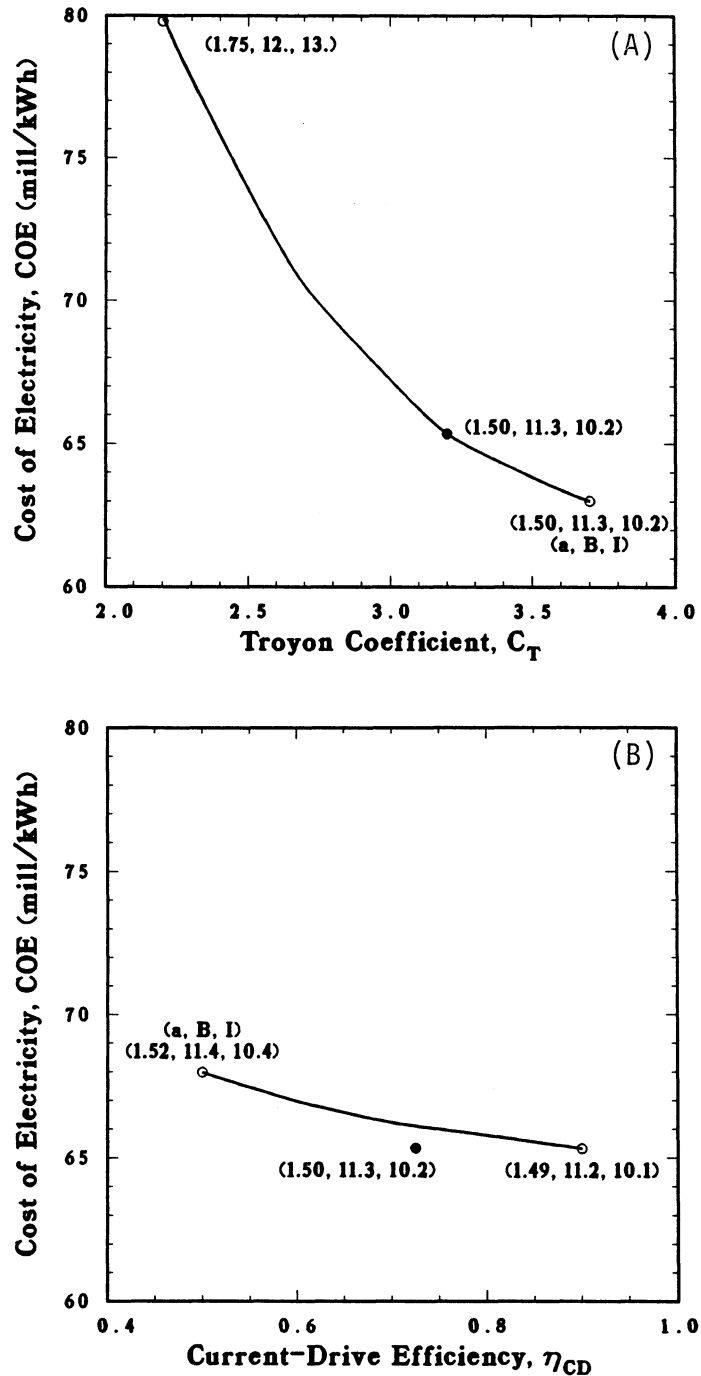


Figure 2.4-8. Projected COE as a function of (A) Troyon coefficient, and (B) FWCD system “wall-plug” efficiency ($P_E = 1000$ MWe, $B_{\phi c} = 21$ T, $\sigma_{all} = 1000$ MPa, $f_{BC} = 0.68$, $\gamma^* = 0.33 \times 10^{20}$ A/W-m², and $A = 4.5$). The ARIES-I design point is denoted by the filled circle.

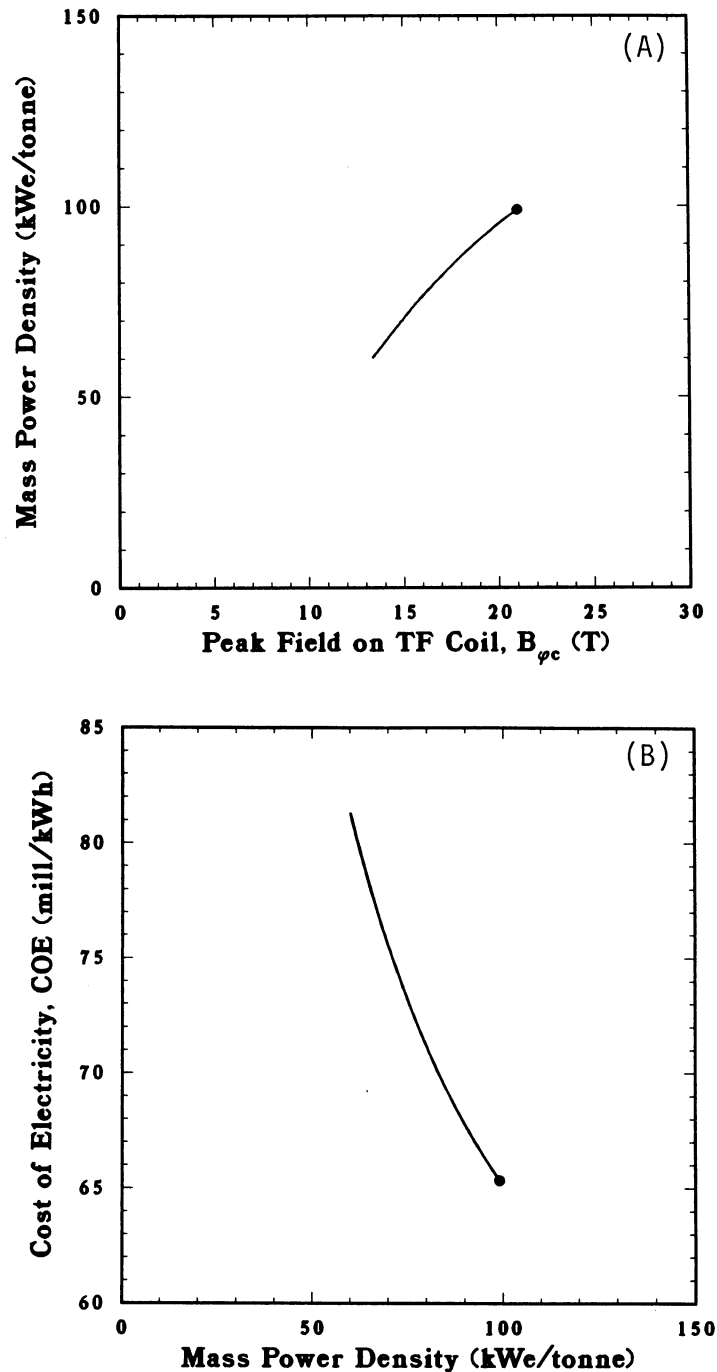


Figure 2.4-9. (A) The MPD as a function of peak TF-coil field strength; and (B) Projected COE as function of MPD ($P_E = 1000$ MWe, $B_{\phi c} = 21$ T, $\sigma_{all} = 1000$ MPa, $f_{BC} = 0.68$, $\gamma^* = 0.33 \times 10^{20}$ A/W-m², and $A = 4.5$). The ARIES-I design point is denoted by the filled circle.

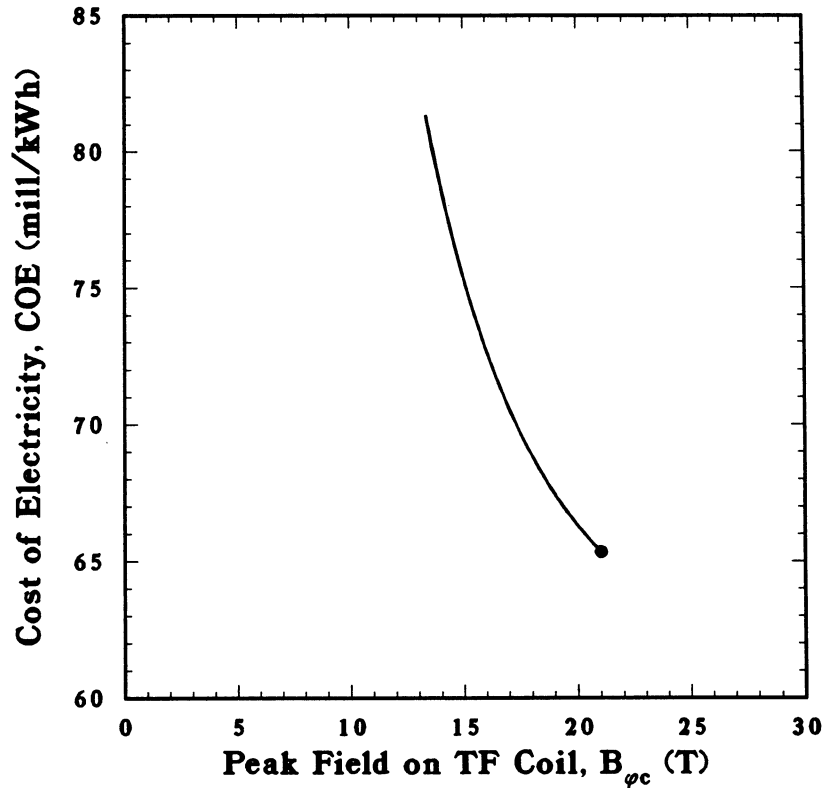


Figure 2.4-10. Projected COE as a function of peak TF-coil field strength ($P_E = 1000$ MWe, $\sigma_{all} = 1000$ MPa, $f_{BC} = 0.68$, $\gamma^* = 0.33 \times 10^{20}$ A/W-m², and $A = 4.5$). The ARIES-I design point is denoted by the filled circle.

In terms of confinement physics extrapolation, the ARIES-I design point is displayed in Fig. 2.4-12 for a range of confinement-time enhancement factors, $H^j \equiv \tau_E/\tau_E^j$, obtained by applying a number of proposed semi-empirical scaling relations [5, 16]. Included are the relations proposed by Goldston, Kaye and Goldston, Kaye (Kaye-Big, Kaye-All), Rebut and Lallia, Riedel and Kaye, Odajima and Shimomura (JAERI), together with ITER power law (ITER89-P) and offset linear (ITER89-OL) scaling [5]. The required enhancement factor ranges from ~ 1.8 to 3.3 as shown for the nominal ARIES-I confinement time, $\tau_E = 2.4$ s at $f_{RAD} = 0.5$. It should be noted that several of the relations predict more required enhancement at larger values of a (*i.e.*, lower B_ϕ).

The ARIES-I study explores one of the possible approaches for improving conventional DT-tokamak reactor performance and in order to reduce the current-drive power requirements of steady-state operation [85, 86]. It is not possible to present here a comprehensive exposition of every parametric study performed that led to the selection of the reference ARIES-I conceptual design point. Nor is it claimed that all potential sensi-

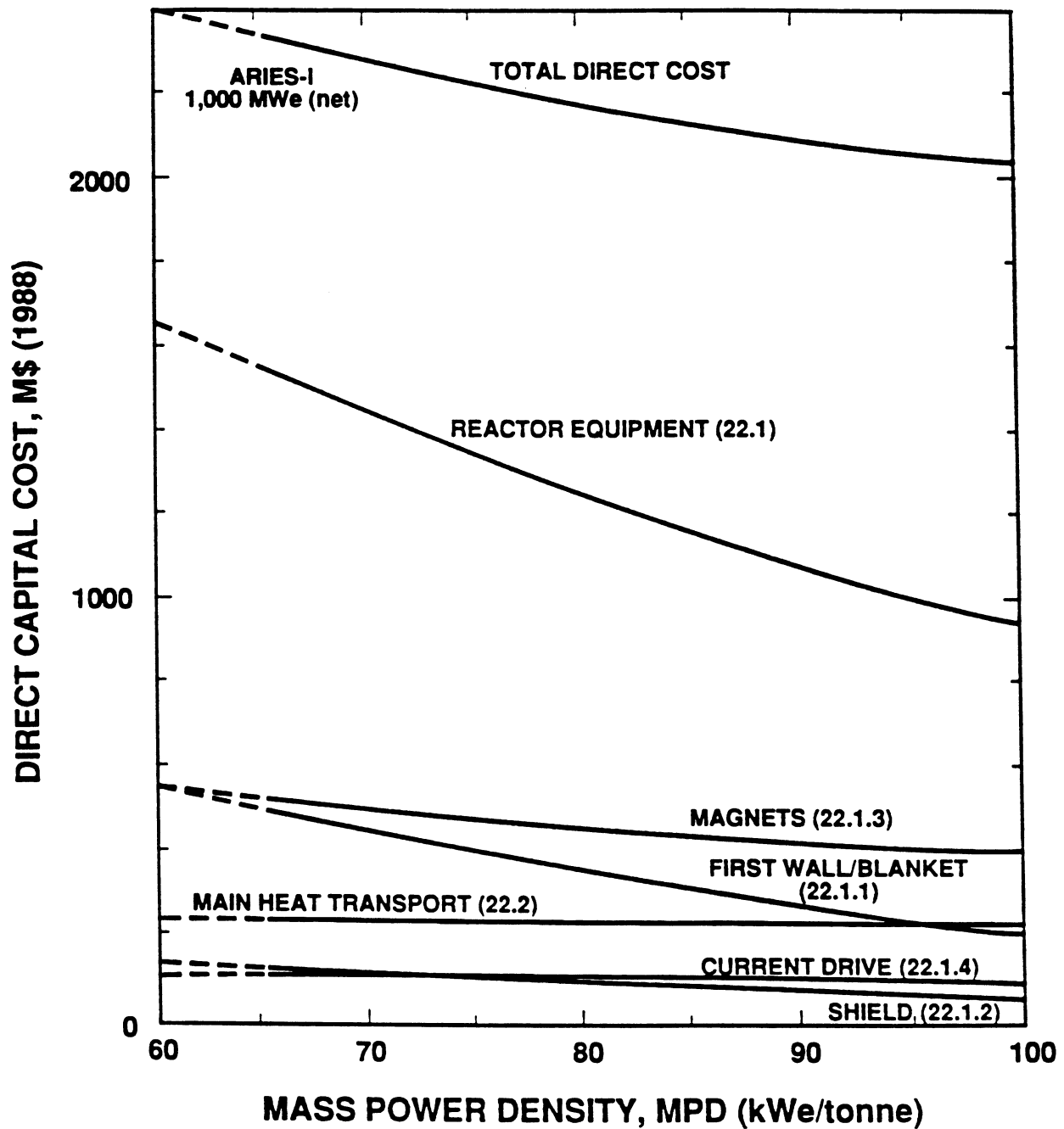


Figure 2.4-11. The direct costs of major reactor components as functions of the MPD figure of merit, reflecting higher peak TF-coil field at higher MPD ($P_E = 1000$ MWe, $\sigma_{all} = 1000$ MPa, $f_{BC} = 0.68$, $\gamma^* = 0.33 \times 10^{20}$ A/W-m², and $A = 4.5$).

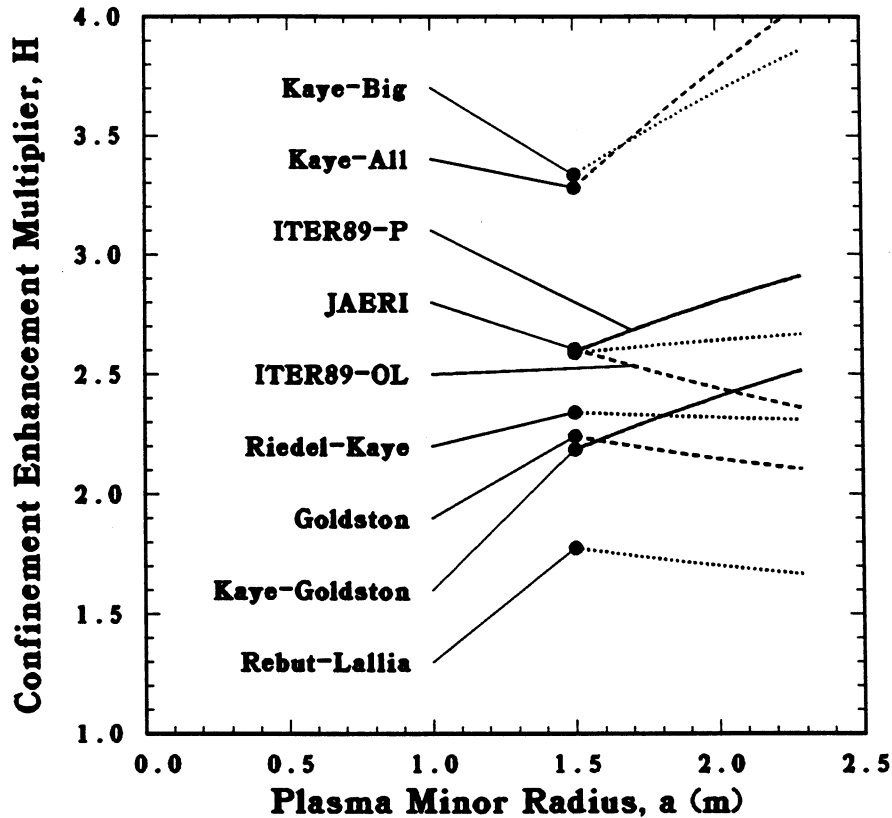


Figure 2.4-12. The variation of ARIES-I confinement-time enhancement factor for a range of proposed, semi-empirical scaling relations [5, 16]. The ARIES-I design point at $a = 1.50$ m, $I_\phi = 10.2$ MA, and $B_{\phi c} = 11.3$ T is denoted by the set of filled circles.

tivities have been exhaustively explained. Rather, an attractive design window for first-stability tokamak reactor operation has been identified. Tokamaks in this design window operate with a relatively high aspect ratio, low plasma current, and high magnetic field. Future technical development and physics optimization can exploit this approach.

2.4.4. ARIES-I Reference Design

The interaction of the parametric modeling described in Sec. 2.4.3, and the detailed design activities of the ARIES project as a whole, led to the selection of the ARIES-I reference design, as summarized in Table 2.4-II. The nominal net electrical power output is $P_E = 1000$ MWe; the plasma aspect ratio is $A = 4.5$ at a major toroidal plasma radius of $R_T = 6.75$ m; the peak TF-coil magnetic field is $B_{\phi c} = 21$ T; and the Troyon-limited toroidal beta is $\beta \simeq 1.9\%$ leading to a modest plasma current of $I_\phi = 10.2$ MA and current-drive power, $P_{CD} \simeq 97$ MW. The recirculating power frac-

Table 2.4-II.
Parameters of the ARIES-I First-Stability Tokamak Reactor

Aspect ratio, $A = R_T/a$	4.5
Major toroidal radius, R_T (m)	6.75
Plasma minor half width, a (m)	1.50
Plasma vertical elongation, $\kappa = b/a$	1.8
Plasma-edge safety factor, q	4.50
Troyon coefficient, C_T	0.032
Plasma toroidal beta, β	1.92%
Plasma temperature, $T_e \simeq T_i$ (keV)	20
Plasma ion density, n_i ($10^{20}/\text{m}^3$)	1.24
Plasma electron density, n_e ($10^{20}/\text{m}^3$)	1.45
Lawson parameter, $n_i\tau_E$ (10^{20} s/ m^3)	2.9
Goldston confinement-time multiplier, H_G	2.2
ITER-89P confinement-time multiplier, H_{89P}	2.6
Plasma Q -value, $Q_p = P_F/P_{CD}$	19.9
On-axis toroidal magnetic field, B_{ϕ_0} (T)	11.3
Peak TF-coil magnetic field, B_{ϕ_c} (T)	21.0
Stored magnetic energy, $W_{B\phi}$ (GJ)	132
Plasma toroidal current, I_ϕ (MA)	10.2
Bootstrap-current fraction, f_{BC}	0.68
Current-drive efficiency, γ (10^{20} A/W- m^2) [A/W]	0.33 [0.034]
Absorbed current-drive power, P_{CD} (MW)	97
14.1-MeV-neutron wall loading, I_w (MW/ m^2)	2.5
Fusion power, P_F (MW)	1,925
Thermal power, P_{TH} (MW)	2,544
Gross electric power, P_{ET} (MW)	1,246
Net electric power output, P_E (MW)	1,000
Recirculating power fraction, $1/Q_E$	0.198
Magnet costs (M\$)	392
Current-drive costs (M\$)	104
First-wall/blanket/shield costs (M\$)	338
Total direct cost, TDC (M\$)	2,140
Unit direct cost, UDC (\$/kWe)	2,140
Total cost (M\$)	3,617
Cost of electricity, COE (mill/kWh)	65.3
Mass power density, MPD (kWe/tonne)	99

tion is $\epsilon = 1/Q_E \simeq 20\%$; the average neutron wall load is $I_w \simeq 2.5 \text{ MW/m}^2$; the MPD is 99 kWe/tonne; and the projected COE is $\sim 65 \text{ mill/kWh}$, using “standard” financial assumptions. For comparison, the corresponding values for “median-experience” and “better experience” fission pressurized-water reactors ($P_E = 1100 \text{ MWe}$) are 78 and 46 mill/kWh, respectively, developed on the same cost-accounting basis. Coal-fired plants ($P_E = 2 \times 550 \text{ MWe}$) costs are projected at 50 mill/kWh [56, 87]. The cost of the ARIES-I reactor are summarized on Table 2.4-III.

Standard assumptions (Sec. 2.3) regarding construction time ($\tau_c = 6 \text{ y}$), plant availability ($p_f = 0.76$), economies of scale, and operation and maintenance charges are used to estimate the constant-dollar (1988) COE. The sensitivity of ARIES-I costs to assumed construction time, τ_c , is summarized in Table 2.4-IV. Without developing a detailed construction schedule, the ARIES-I lead time is taken to be six years, in common with the times of the STARFIRE [54], MARS [60], and TITAN [2] studies.

Figure 2.4-13 summarizes the ARIES-I design space and exhibits the economy of scale associated with plant size. Reactors to the left of the chain-dashed line are physically smaller and have higher neutron wall load and MPD, but require technology beyond that of ARIES-I to achieve $B_{\phi c} \geq 21 \text{ T}$. The incremental COE savings at higher P_E , taking advantage of the economies of scale, implies more severe divertor-plate loads.

In the cost estimates for ARIES-I, no safety-assurance cost credits [37] have been taken, which may be expected to result from the use of low-activation materials. These credits lower the reported COE by 20% to 25%, as suggested in Table 2.4-V, by using the passive-safety cost credits summarized in Table 2.3-VI. A more restrictive application of the passive-safety cost credits (which retains N-stamp costs for the TF coils, blanket, and main heat-transport system) results in a more modest $\sim 14\%$ reduction in projected COE.

To summarize ARIES-I costs, Fig. 2.4-14 displays estimated COE as a function of peak TF-coil magnetic-field strength, $B_{\phi c}$. The nominal ARIES-I TF-coil unit cost is \$90/kg. The impact of different TF-coil unit costs are also shown. For comparison, a conceptual 1000-MWe ITER extrapolation ($A \simeq 3$) using nearer-term 14-T TF coils, consistent with Refs. [88] and [89], are shown with COE $\simeq 90 \text{ mill/kWh}$. ARIES-I represents a significant improvement of the tokamak approach, given the availability of high field-coil technology and physics performance with high radiation fraction, $f_{RAD} = 0.5$, and large bootstrap-current contribution, $f_{BC} = 0.68$. Also, a preliminary result for the second-stability-regime ARIES-II ($\beta \simeq 16\%$) is included, although work on this tokamak approach is ongoing [11] and COE values may change.

Table 2.4-III.
ARIES-I Systems-Code Cost Summary (1988 \$)

Acct. No.	Account Title	Million Dollars
20.	Land and land rights	5.3
21.	Structures and site facilities	339.3
22.	Reactor plant equipment (RPE)	1,362.8
22.1.1	Blanket and first wall	260.3
22.1.2	Shield	77.3
22.1.3	Magnets	392.3
22.1.4	Supplemental heating systems (current drive)	103.9
22.1.5	Primary structure and support	63.6
22.1.6	Reactor vacuum systems (unless integral elsewhere)	32.2
22.1.7	Power supply, switching, and energy storage	51.3
22.1.8	Impurity control	7.9
22.1.9	Direct energy conversion system	N/A
22.1.10	ECRH breakdown system	23.0
22.1	Reactor equipment	1,011.8
22.2	Main heat transfer and transport system	229.7
23.	Turbine plant equipment	245.3
24.	Electric plant equipment	137.1
25.	Miscellaneous plant equipment	50.5
26.	Special materials	0.6
90.	Total direct cost	2,140.7
91.	Construction services and equipment (10%)	214.1
92.	Home office engineering and services (10%)	214.1
93.	Field office engineering and services (10%)	214.1
94.	Owner's costs (5%)	107.0
96.	Project contingency (10%)	214.1
97.	Interest during construction (IDC)	512.8
98.	Escalation during construction (EDC)	0.
99.	Total capital cost	3,616.9
		<u>Constant Dollars</u>
[90]	Unit direct cost, UDC (\$/kWe)	2,140.8
[94]	Unit base cost, UBC (\$/kWe)	3,104.1
[99]	Unit total cost, UTC (\$/kWe)	3,616.9
	Capital return (mill/kWh)	52.6
[40-47,51]	O&M (1.4%) (mill/kWh)	6.7
[50]	First-wall/blanket replacement (mill/kWh)	5.6
	Decommissioning allowance	0.5
[02]	Deuterium fuel (mill/kWh)	0.04
	Cost of electricity, COE (mill/kWh)	65.3

Table 2.4-IV.
Impact of Construction Lead Time^(a)

Lead Time (y)	<i>f_{IDC}</i>	Total Cost (M\$)	COE (mill/kWh)
4	0.1118	3,451	62.9
5	0.1381	3,533	64.1
6 ^(b)	0.1652	3,617	65.3
7	0.1931	3,703	66.6
8	0.2219	3,793	67.9
9	0.2515	3,885	69.2
10	0.2821	3,980	70.6

^(a)For all cases, the total direct cost is \$2,141 M (1988).

^(b)ARIES-I base case.

Table 2.4-V.
Impact of Safety-Assurance Cost Credits on COE (mill/kWh)^(a)

	Base Case ^(b)	Option-1	Option-2
Capital return	52.6	37.7	43.5
Operation and maintenance	6.7	6.7	5.1
First-wall/blanket replacement	5.6	2.8	5.0
Decommissioning	0.5	0.5	0.5
Fuel	0.04	0.04	0.04
Total COE	65.3	47.7	54.1

^(a)cf., Table 2.3-VI.

^(b)ARIES-I without passive-safety credits.

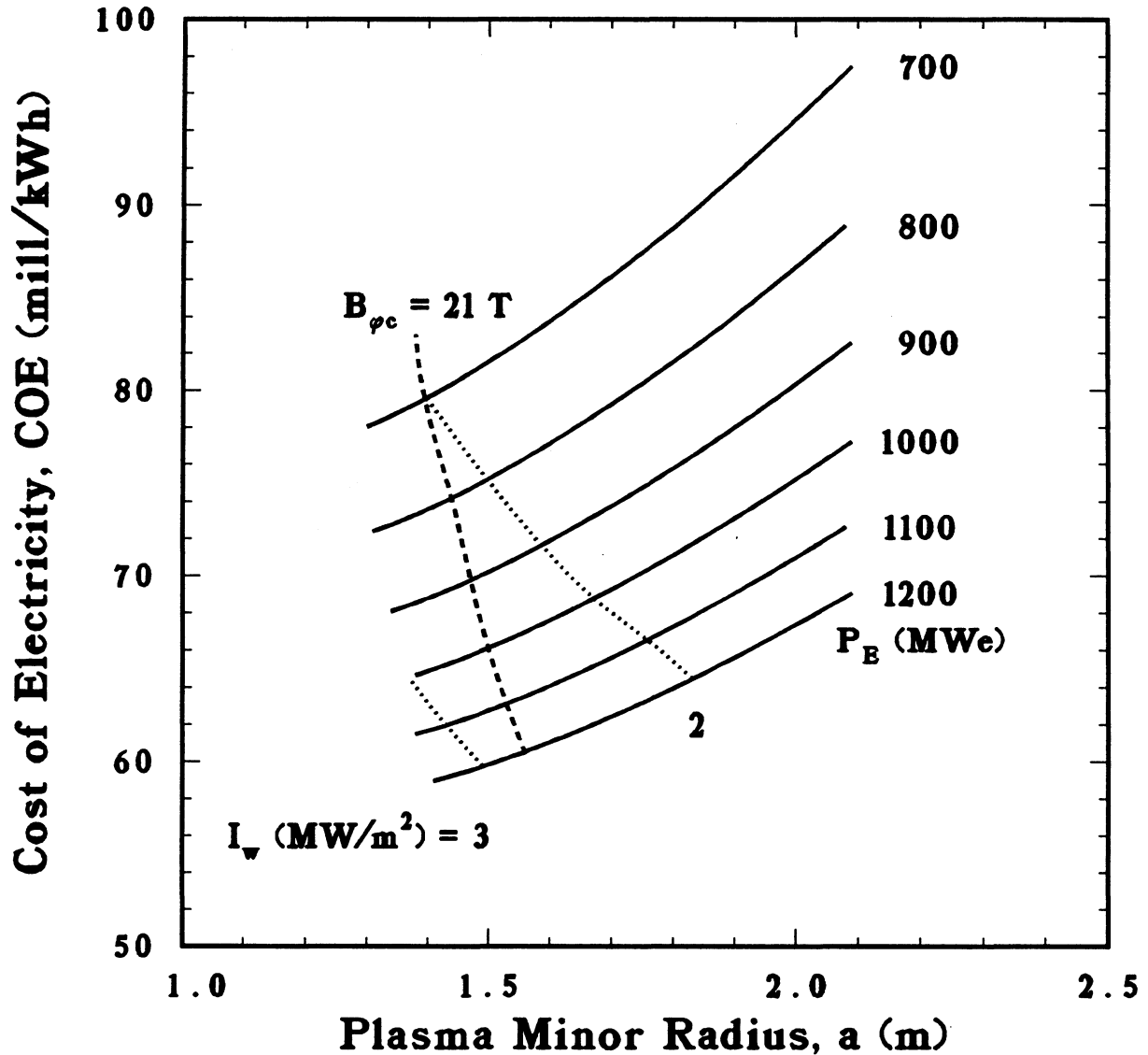


Figure 2.4-13. The COE as a function of plasma minor radius for fixed plasma aspect ratio, $A = 4.5$ and the other indicated fixed parameters. Curves of constant net electrical power output, P_E , are shown. Contours of fixed average neutron wall load, I_w , are included. The boundary with peak TF-coil field strength, $B_{\phi c} = 21 \text{ T}$, is also included, restricting access to small values of a .

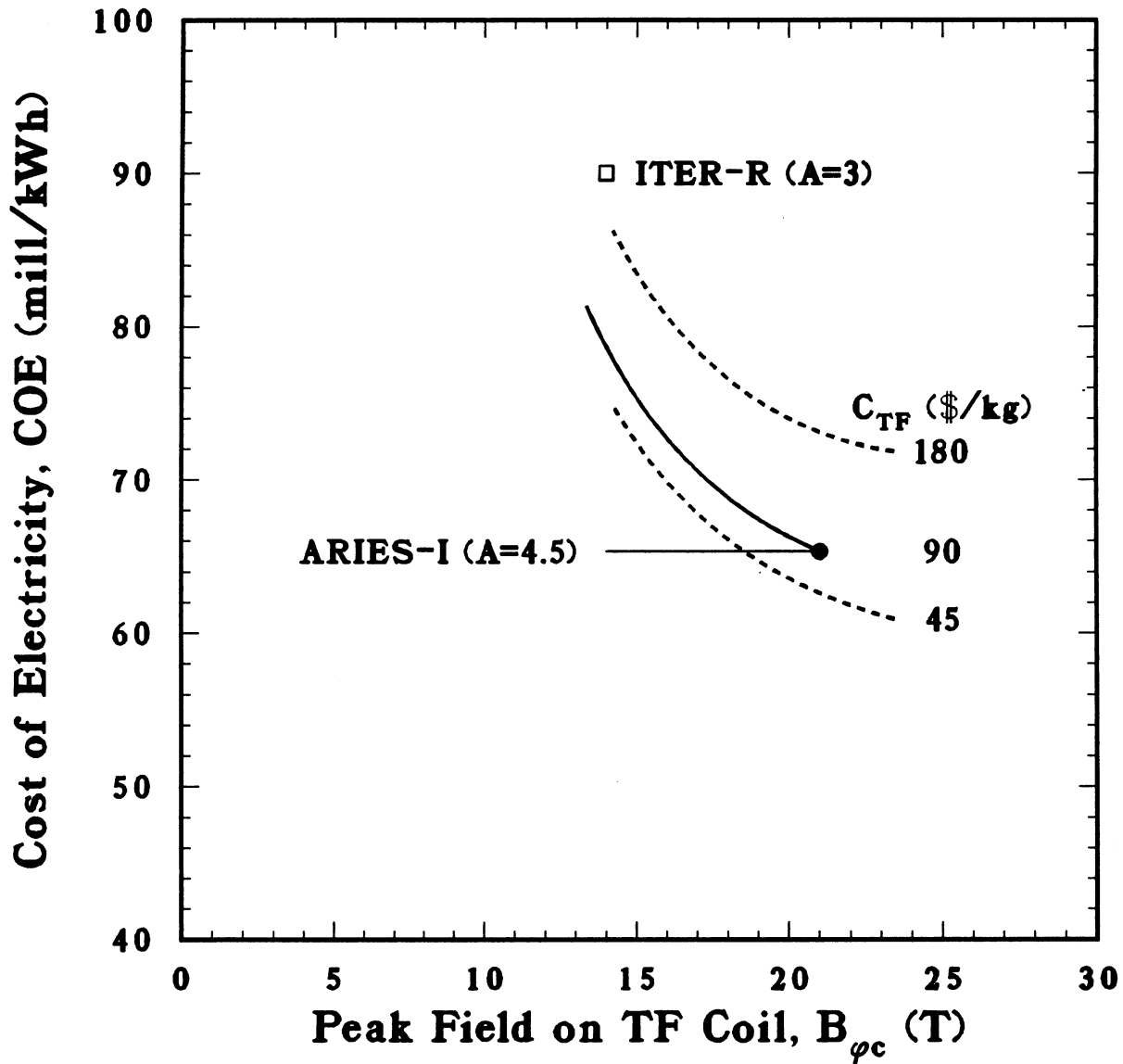


Figure 2.4-14. Dependence of COE on peak TF-coil magnetic-field strength, for ARIES-I assuming various TF-coil unit costs, C_{TF} . A conceptual ITER-reactor extrapolation and a preliminary second-stability ARIES-II case are also included.

2.5. CRITICAL ISSUES

In addition to the engineering feasibility of various subsystems, the following issues impact the selection of cost-optimized design points:

1. The cost of fabricating large SiC-composite components (assumed to be \$400/kg for ARIES-I blanket and \$50/kg for bulk SiC shield, as described in Sec. 8.2.5);
2. The cost of balance of plant for achieving the gross thermal efficiency of 49% (650°C and 10-MPa helium coolant with a primary heat-transport cost of \$0.09/Wt, and 650°C steam-turbine plant equipment at \$0.20/We);
3. The cost of zirconium isotope separation needed for Li_2ZrO_3 breeder (\$2000/kg as described in Sec. 10.4.1) and for cost implication of other low-activation breeders (*e.g.*, Li_2O , Li_4SiO_4);
4. The economic impact (from resource, safety, and environmental viewpoints) of using large quantities of Be;
5. Realization of plant availability of 0.76.

The ARIES-I design reflects major improvements when compared with past “conventional” tokamak reactor studies: The reactor cost is reduced by a factor two and, at the same time, significant advances in physics realism are achieved and dramatic improvement in safety and environmental attributes are made. This reduction in cost is mostly due to the advanced fusion-power core of ARIES-I (advanced high-field superconducting magnet and SiC-composite structural material). The ARIES-I cost of electricity (COE) is projected at 65.3 mill/kWh, which is comparable to median-experience fission reactors but more expensive than best-experience advanced-fission or coal power plants (not including external, hidden costs associated with the use of both fission and fossil fuels). It is expected that potential advances in tokamak physics, such as the second stability operation, can improve the economics of tokamak reactors. The ARIES-II design will explore this region of tokamak operation.

2.6. SUMMARY AND CONCLUSIONS

The ARIES-I cost-optimized design point is the result of a symbiotic integration of physics, engineering, and power economics. The systems model has received continual input and updating from the conceptual detailed engineering-design activity. While

many of the physics and engineering models are simplified, the result, nevertheless, has been the first self-consistent tokamak power-reactor study to include the quantitative interdependence of equilibrium/stability, current drive, impurity control, transport in high-radiation tokamak plasmas, *etc.*, while simultaneously providing realistic and detailed cost projections using a modern methodology that is presently being used to assess a broad spectrum of nuclear and fossil energy sources.

The attractiveness of the first-stability ARIES-I tokamak reactor, as measured by COE and related figures of merit (*e.g.*, MPD and Q_E) has been achieved through

1. Operation at high aspect ratio ($A = 4.5$) and low plasma current ($I_\phi = 10.2$ MA) to increase the poloidal beta and obtain a high bootstrap-current fraction of 68%. This approach minimizes the current-drive power and maximizes the engineering Q -value ($Q_E = 5.1$).
2. Trade-off of plasma aspect ratio with current to limit the required confinement enhancement factor ($H = 1.8 - 3.3$, depending on the specific scaling considered).
3. Use of advanced TF coils (ternary Nb_3Sn operated at 21 T) with a stabilizer that carries structural load and unique structural cup to carry overturning moments. The high toroidal field is used to compensate for the low toroidal beta (1.9%) to achieve an acceptable plasma fusion-power density (3.9 MW/m³) and a mass power density of 100 kWe/tonne of FPC.

REFERENCES

- [1] R. L. Miller, R. A. Krakowski, C. G. Bathke, C. Copenhaver, N. M. Schnurr, A. G. Engelhardt, T. J. Seed, and R. M. Zubrin, "Advanced Tokamak Reactors Based on the Spherical Torus (ATR/ST)," Los Alamos National Laboratory report LA-10740-MS (1986).
- [2] F. Najmabadi, R. W. Conn, R. A. Krakowski, K. R. Schultz, D. Steiner, and the TITAN Research Group, "The TITAN Reversed-Field-Pinch Reactor Study—The Final Report," University of California Los Angeles, General Atomics, Los Alamos National Laboratory, and Rensselaer Polytechnic Institute, University of California Los Angeles report UCLA-PPG-1200 (1990); also, F. Najmabadi, R. W. Conn, R. A. Krakowski, K. R. Schultz, D. Steiner, and the TITAN Research Group, "Engineering and Physics of High-Power-Density, Compact, Reversed-Field-Pinch Fusion Reactors: The TITAN Study," *Proc. 15th Symp. Fusion Technol. (SOFT)*, Utrecht, the Netherlands (Sept. 1988), *Fusion Technology 88*, A. M. Van Ingen, A. Nijssen-Vis, H. T. Klippel, Eds., North-Holland, Amsterdam (1989) p. 1779.
- [3] M. E. Fenstermacher, "MUMAK—A Computer Code for Modeling Plasma Power Balance and Current Drive in Tokamaks," Lawrence Livermore National Laboratory report UCID-21038 (1987).
- [4] M. E. Fenstermacher, R. S. Devoto, R. H. Bulmer, J. D. Lee, J. R. Miller, and J. H. Schultz, "A Non-Inductively Driven Tokamak Reactor Based on ITER," *Fusion Technol.* **15** (1989) 740.
- [5] "ITER Conceptual Design Report," ITER Documentation Internal Series No. 7, International Atomic Energy Agency, Vienna (1989).
- [6] W. M. Stacey, V. A. Maroni, J. R. Purcell, *et al.*, "Tokamak Experimental Power Reactor Studies," Argonne National Laboratory report ANL/CTR-75-2 (1975).
- [7] D. A. Ehst, K. Evans, Jr., and W. M. Stacey, Jr., "The Influence of Physics Parameters on Tokamak Reactor Design," *Nucl. Technol.* **43** (1979) 28.
- [8] P. I. H. Cooke, R. Hancox, and W. R. Spears, "Parameters of a Reference Tokamak Reactor," UKAEA Culham Laboratory report CLM-R298 (1989).
- [9] J. Sheffield, R. A. Dory, S. M. Cohn, J. G. Delene, L. Parsly, D. E. T. F. Ashby, and W. T. Reiersen, "Cost Assessment of a Generic Magnetic Fusion Reactor," *Fusion Technol.* **9** (1986) 199.

- [10] J. G. Delene, R. A. Krakowski, J. Sheffield, and R. A. Dory, "GENEROMAK Fusion Physics, Engineering, and Costing Model," Oak Ridge National Laboratory report ORNL/TM-10728 (1988).
- [11] R. L. Miller, W. R. Spears, R. Hancox, and R. A. Krakowski, "Comparison of EURATOM and U.S. Estimates of Fusion Reactor Costs," *Proc. of ANS 9th Top. Mtg. Technol. of Fusion Energy*, Oak Brook, IL (Oct. 1990) *Fusion Technol.* **19** (1991) 813.
- [12] K. A. Werley, "Reversed Field Pinch Ignition Physics," Los Alamos National Laboratory report LA-UR-89-4093 (1989) (submitted to *Nucl. Fusion*).
- [13] W. Kernbichler, "Fuel Alternatives in Nuclear Fusion," Ph.D. thesis, Graz University of Technology, Austria (1987).
- [14] W. Kernbichler, G. H. Miley, and M. Heindler, "D-³He Fuel Cycles for Neutron Lean Reactors," *Fusion Technol.* **15** (1989) 1142.
- [15] W. Kernbichler, G. H. Miley, and M. Heindler, "Comparison of the Physics Performance of D-³He Fusion in High- and Low-Beta Toroidal Devices," *Proc. 5th Int. Conf. on Emerging Nucl. Energy Systems*, Karlsruhe, Germany (July 1989) 192.
- [16] N. A. Uckan, "ITER Physics Design Guidelines Version-1," ITER report ITER-TN-PH-8-6, International Atomic Energy Agency, Vienna (1988).
- [17] J. D. Galambos and Y-K. M. Peng, "Ignition and Burn Criteria for D-³He Tokamak and Spherical Torus Reactors," Oak Ridge National Laboratory report ORNL/P-89/2554 (1989) (submitted to *Fusion Technol.*).
- [18] J. P. Freidberg and J. A. Wesson, "Minimum Required Beta in a Tokamak Reactor," *Nucl. Fusion* **25** (1985) 759.
- [19] C. A. Flanagan, D. Steiner, G. E. Smith, *et al.*, "Initial Trade and Design Studies for the Fusion Engineering Device," Oak Ridge National Laboratory report ORNL/TM-7777 (1981).
- [20] F. Troyon, R. Gruber, H. Sauernmann, S. Semenzato, and S. Succi, "MHD-Limits to Plasma Confinement," *Plasma Phys. Controlled Fusion* **26** (1984) 209.
- [21] J. R. McNally, Jr., "Physics of Fusion Fuel Cycles," *Nucl. Technol./Fusion* **2** (1982) 9.

- [22] R. A. Krajcik, "The Effect of a Metallic Reflector Upon Cyclotron Radiation," *Nucl. Fusion* **13** (1973) 7.
- [23] M. Schaffer, "Synchrotron Radiation Power Loss and Implications for ARIES Reactors," General Atomics, ARIES Program internal memo (Jan. 1989).
- [24] K. A. Werley, Los Alamos National Laboratory, private communication (April 1989).
- [25] S. Tamor, "Calculation of Energy Transport by Cyclotron Radiation in Fusion Plasmas," *Nucl. Technol./Fusion* **3** (1983) 293.
- [26] L. M. Hively, "Convenient Computational Forms for Maxwellian Reactivities," *Nucl. Fusion* **17** (1977) 873.
- [27] S. L. Greene, Jr., "Maxwell Averaged Cross Sections for Some Thermonuclear Reactions on Light Isotopes," Lawrence Radiation Laboratory report UCRL-70522 (1967).
- [28] N. Jarmie, R. E. Brown, and R. A. Hardenkopf, "Fusion-Energy Reaction ${}^2\text{H}(t, \alpha)n$ from $E_t = 12.5$ to 117 keV," *Phys. Rev. C* **29** (1984) 2031; also relevant Erratum in *Phys. Rev. C* **33** (1986) 385.
- [29] P. I. H. Cooke, UKAEA Culham Laboratory, private communication (1989).
- [30] B. J. Braams, "A Multi-Fluid Code for Simulation of the Edge Plasma in Tokamaks," NET report NET-68, EUR-FU/XII-80/87/68 (1987).
- [31] P. J. Harbour, "Thickness of the Scrape-off Layer of a Large Tokamak with a Poloidal Divertor," *Nucl. Fusion* **24** (1984) 1211.
- [32] N. A. Uckan, "Tokamak Confinement Projections and Performance Goals," *Fusion Technol.* **15** (1989) 391.
- [33] M.-Y. Hsiao, D. A. Ehst, and K. Evans, Jr., "Bootstrap Currents in Radio-Frequency Driven Tokamak Equilibria," *Nucl. Fusion* **29** (1989) 49.
- [34] B. Q. Deng and G. A. Emmert, "Fast Ion Pressure in Fusion Plasmas," University of Wisconsin report UWFD-718 (1987).
- [35] L. R. Turner and M. A. Abdou, "Computational Model for Superconducting Toroidal-Field Magnets for a Tokamak Reactor," Argonne National Laboratory report ANL/FPP/TM-88 (1977).

- [36] J. Schwartz, J. R. Miller, and J. E. C. Williams, "TF Overall Current Density Scaling," Massachusetts Institute of Technology, ARIES Program internal memo (Nov. 1988).
- [37] J. P. Holdren, D. H. Berwald, R. J. Budnitz, J. G. Crocker, J. G. Delene, R. D. Endicott, M. S. Kazimi, R. A. Krakowski, B. G. Logan, and K. R. Schultz, "Report of the Senior Committee on Environmental, Safety, and Economic Aspects of Magnetic Fusion Energy," Lawrence Livermore National Laboratory report UCRL-53766 (1989); also, J. P. Holdren, D. H. Berwald, R. J. Budnitz, J. G. Crocker, J. G. Delene, R. D. Endicott, M. S. Kazimi, R. A. Krakowski, B. G. Logan, and K. R. Schultz, "Exploring the Competitive Potential of Magnetic Fusion Energy: The Interaction of Economics with Safety and Environmental Characteristics," *Fusion Technol.* **13** (1988) 7.
- [38] R. A. Krakowski and J. G. Delene, "Connections Between Physics and Economics for Tokamak Fusion Power Plants," *J. Fusion Energy* **7** (1988) 49.
- [39] R. J. Roark and W. C. Young, *Formulas for Stress and Strain*, 5th ed., McGraw-Hill, New York (1982) p. 556.
- [40] S. Timoshenko and J. N. Goodier, *Theory of Elasticity*, 2nd ed., McGraw-Hill, New York (1951).
- [41] D. J. Strickler, J. B. Miller, K. E. Rothe, and Y.-K. M. Peng, "Equilibrium Modeling of the TFCX Poloidal Field Coil System," Oak Ridge National Laboratory report ORNL/FEDC-83/10 (1984).
- [42] C. G. Bathke, S. C. Jardin, J. A. Leuer, and D. J. Ward, "Vertical Stability Requirements for ARIES-I Reactor," *Proc. IEEE 13th Symp. on Fusion Eng.*, Knoxville, TN (Oct. 1989), IEEE No. 89CH2820-9, IEEE, Piscataway, NJ (1990) p. 909.
- [43] H. M. Attaya and M. E. Sawan, "NEWLIT-A General Code for Neutron Wall Loading Distribution in Toroidal Reactors," *Fusion Technol.* **8** (1985) 609.
- [44] R. W. Conn (Chairman), "Panel X Report to the U.S. Department of Energy Magnetic Fusion Advisory Committee" (May 1985).
- [45] M. A. Abdou, M. S. Tillack, A. R. Raffray, *et al.*, "Modeling, Analysis and Experiments for Fusion Nuclear Technology FNT Progress Report: Modeling & FINESSE," University of California Los Angeles report UCLA-PPG-1021 (1987) 2.

- [46] D. L. Smith, G. D. Morgan, *et al.*, "Blanket Comparison and Selection Study—Final Report," Argonne National Laboratory report ANL/FPP-84-1 (1984).
- [47] S. L. Thomson, "Cost Algorithms for Superconducting Magnets," Oak Ridge National Laboratory report FEDC-M-88-ITER-001 (1988).
- [48] R. L. Reid and W. R. Becraft, Oak Ridge National Laboratory, private communication (April 1989).
- [49] W. R. Hamilton, D. C. Keeton, and S. L. Thomson, "Cost Accounting System for Fusion Studies," Oak Ridge National Laboratory report ORNL/FEDC-85/7 (1985).
- [50] S. C. Schulte, T. L. Wilke, and J. R. Young, "Fusion Reactor Design Studies—Standard Accounts for Cost Estimates," Battelle Pacific Northwest Laboratory report PNL-2648 (1978).
- [51] D. L. Phung, "A Method for Estimating Escalation and Interest During Construction (EDC and IDC)," in *Proc. 2nd Miami Conf. on Alternative Energy Sources*, Miami, FL (Dec. 1979).
- [52] S. L. Thomson, "Reference Cost Data for Fusion," Oak Ridge National Laboratory report ORNL/FEDC-86-8 (1986).
- [53] S. C. Schulte, W. E. Bickford, C. E. Willingham, S. K. Ghose, and M. G. Walker, "Fusion Reactor Design Studies—Standard Unit Costs and Cost Scaling Rules," Pacific Northwest Laboratory report PNL-2987 (1979).
- [54] C. C. Baker, M. A. Abdou, R. M. Arons, A. E. Bolon, C. D. Boley, J. N. Brooks, *et al.*, "STARFIRE—A Commercial Tokamak Fusion Power Plant Study," Argonne National Laboratory report ANL/FPP-80-1 (1980).
- [55] L. Argote and D. Epple, "Learning Curves in Manufacturing," *Science* **247** (1990) 920.
- [56] J. G. Delene, K. A. Williams, and B. H. Shapiro, "Nuclear Energy Cost Data Base," U.S. Department of Energy report DOE/NE-0095 (1988).
- [57] "MINIMARS Conceptual Design: Final Report," J. D. Lee, Ed., Lawrence Livermore National Laboratory report UCID-20773 (1986).
- [58] I. Maya, K. R. Schultz, R. F. Bourque, E. T. Cheng, R. L. Creedon, J. H. Norman, *et al.*, "Inertial Confinement Fusion Reaction Chamber and Power Conversion System Study," General Atomics report GA-A17842 (1985).

- [59] B. Badger, I. N. Sviatoslavsky, S. W. Van Sciver, G. L. Kulcinski, G. A. Emmert, D. T. Anderson, *et al.*, "UWTOR-M: A Conceptual Modular Stellarator Power Reactor," University of Wisconsin report UWFDM-550 (1982).
- [60] B. G. Logan, C. D. Henning, G. A. Carlson, R. W. Werner, D. E. Baldwin, W. L. Barr, *et al.*, "MARS Mirror Advanced Reactor Study Final Report," Lawrence Livermore National Laboratory report UCRL-53480 (1984).
- [61] J. G. Delene, "Operation and Maintenance Cost Estimate for Fusion Power Plants," Oak Ridge National Laboratory, unpublished data (Feb. 1989).
- [62] J. G. Delene, "GENEROMAK Model Update," Oak Ridge National Laboratory, unpublished data (Feb. 1989).
- [63] N. J. Fisch, "Theory of Current Drive in Plasmas," *Rev. Mod. Phys.* **59** (1987) 175.
- [64] D. A. Ehst and K. Evans, Jr., "Multiple Wave RF Current Driven Tokamak Reactors in the First Stability Regime," *Nucl. Fusion* **27** (1987) 1267.
- [65] N. J. Fisch, "Confining a Tokamak Plasma with RF-Driven Currents," *Phys. Rev. Lett.* **41** (1978) 873.
- [66] D. A. Ehst, K. Evans, Jr., and M. Klasky, "RF Generation of Stable High Bootstrap Current Equilibria," *Phys. Rev. Lett.* **64** (1990) 1891.
- [67] S. A. Sabbagh, M. H. Hughes, M. W. Phillips, A. M. M. Todd, G. Navratil, *et al.*, "Transition to the Second Region of Ideal MHD Stability," *Nucl. Fusion* **29** (1989) 423.
- [68] F. X. Söldner, "Control of Plasma Profiles With Lower Hybrid Waves," *Applications of Radio-Frequency Power to Plasmas*, S. Bernabei and R. W. Motley, Eds., American Institute of Physics, New York (1987) p. 102.
- [69] T. C. Simonen, M. Matsuoka, D. K. Bhadra, *et al.*, "Neutral-Beam Current-Driven High-Poloidal-Beta Operation of the DIII-D Tokamak," *Phys. Rev. Lett.* **61** (1988) 1720.
- [70] S. C. Luckhardt, K.-I. Chen, S. Coda, J. Kesner, R. Kirkwood, B. Lane, M. Porkolab, and J. Squire, "Production and Maintenance of High Poloidal Beta Tokamak Plasmas by Means of RF Current Drive," *Phys. Rev. Lett.* **62** (1989) 1508.

- [71] M. C. Zarnstorff, M. G. Bell, M. Bitter, *et al.*, "Bootstrap Current in TFTR," *Phys. Rev. Lett.* **60** (1988) 1306.
- [72] J. G. Cordey, C. D. Challis, and P. M. Stubberfield, "Bootstrap Current Theory and Experimental Evidence," *Plasma Phys. Controlled Fusion* **30** (1988) 1625.
- [73] G. Becker, "Effect of Bootstrap and Beam Driven Currents on Current Profile and Ballooning Stability in ASDEX L- and H-Mode Plasmas," *Nucl. Fusion* **29** (1989) 1291.
- [74] R. L. Miller and the ARIES Team, "The ARIES-I High-Field- Tokamak Reactor: Design-Point Determination and Parametric Studies," *Proc. IEEE 13th Symp. on Fusion Eng.*, Knoxville, TN (Oct. 1989), IEEE No. 89CH2820-9, IEEE, Piscataway, NJ (1990) p. 1027.
- [75] R. Grimm, R. L. Dewar, and J. Manickam, "Ideal MHD Stability Calculations in Axisymmetric Toroidal Coordinate Systems," *J. Comput. Phys.* **49** (1983) 94.
- [76] M. W. Phillips, A. M. M. Todd, M. H. Hughes, *et al.*, "MHD Stability Properties of a High Current, High Beta Tokamak," *Nucl. Fusion* **28** (1988) 1499.
- [77] C. E. Singer, L.-P. Ku, and G. Bateman, "Plasma Transport in a Compact Ignition Tokamak," *Fusion Technol.* **13** (1988) 543.
- [78] T. Yamamoto, H. Aikawa, K. Hoshino, *et al.*, "Improvement of RF Current Drive Density Limit in the JFT-2M Tokamak," *Proc. 12th Int. Conf. on Plasma Phys. and Controlled Nucl. Fusion Research*, Nice, France (Oct. 1988), International Atomic Energy Agency, Vienna (1989) 733.
- [79] Y. Uesugi *et al.*, "Electron Heating and Current Drive By 200 MHz Fast Wave on JFT-2M Tokamak," *Proc. 16th Eur. Conf. on Controlled Fusion and Plasma Phys.*, Venice, Italy (1989), S. Segre, H. Knoepfel, E. Sindoni, Eds., *European Physical Soc.* **13B** (1989) 1259.
- [80] L.-G. Ericksson and T. Hellsten, "Electron Heating During Ion Cyclotron Resonance Heating in JET," *Nucl. Fusion* **29** (1989) 875.
- [81] S. P. Hirshman, "Finite-Aspect-Ratio Effects on the Bootstrap Current in Tokamaks," *Phys. Fluids* **31** (1988) 3150.
- [82] D. A. Ehst, C. D. Boley, and K. Evans, Jr., *et al.*, "Lower Hybrid Heating and Current Drive System for a Tokamak Reactor," *J. Fusion Energy* **2** (1982) 83.

- [83] V. W. Loose and T. Flaim, "Economies of Scale and Reliability: The Economics of Large Versus Small Generating Units," *Energy Systems and Policy* **4** (1980) 37.
- [84] B. I. Spinrad, M. R. Shay, R. P. Jenks, and J. K. Chan, "Effects of Unit Power, Construction Time and Time of Operation on the Capital Costs of LWR Electrical Generating Plants," Oregon State University report OSU-NE-8307 (1983).
- [85] L. Bromberg and D. R. Cohn, "High Field Tokamak Reactors," *Proc. of 4th IAEA Technical Comm. Mtg. and Wkshp. on Fusion Reactor Des. and Technol.*, Yalta, USSR (May-June 1986), International Atomic Energy Agency report IAEA-TC-392.3, Vienna (1987) p. 211.
- [86] J. Schwartz, L. Bromberg, D. R. Cohn, and J. E. C. Williams, "Performance Limits of High Field Tokamak Reactors," *Nucl. Fusion* **29** (1989) 983.
- [87] J. G. Delene, H. I. Bowers, and B. H. Shapiro, "Economic Potential for Future Water Reactors," *Trans. Am. Nucl. Soc.* **57** (1988) 205.
- [88] R. S. Devoto, W. L. Barr, R. H. Bulmer, R. B. Campbell, M. E. Fenstermacher, J. D. Lee, B. G. Logan, J. R. Miller, L. L. Reginato, R. A. Krakowski, R. L. Miller, O. A. Anderson, W. S. Cooper, J. Schultz, J. Yugo, J. H. Fink, and Y. Gohar, "Projections for a Steady-State Tokamak Reactor Based on the International Thermonuclear Experimental Reactor," *Fusion Technol.* **19** (1991) 251.
- [89] C. D. Henning, "ITER in Perspective," *Proc. IEEE 13th Symp. on Fusion Eng.*, Knoxville, TN (Oct. 1989), IEEE No. 89CH2820-9, IEEE, Piscataway, NJ (1990) p. 481.